Supporting Information for

A New Interpretation of Deformation Rates in the Snake River Plain and Adjacent Basin and Range Regions Based on GPS Measurements

S.J. Payne[1], R. McCaffrey[2], R.W. King[3], and S.A. Kattenhorn[4]

[1]Idaho National Laboratory, PO Box 1625, MS 2203, Idaho Falls, ID 83415

[2]Portland State University, Department of Geology, PO Box 751, Portland, OR 97207

[3] Massachusetts Institute of Technology, Department of Earth, Atmospheric & Planetary Sciences, Cambridge, MA 02139

[4]University of Idaho, Department of Geological Sciences, PO Box 443022, Moscow, ID 83844

Geophysical Journal International, 2012

Table of Contents

Calculation of Strain Rates and Slip Rates for Velocity Profiles

Horizontal GPS velocities used to calculate strain and slip rates are listed in Table S-1 and are shown in manuscript Figures 4 and 5. These velocities are different from those listed in Table S-9 because we compute and project components of the velocities that are parallel or perpendicular to the profile lines. To minimize distortion that may occur due to Earth flattening, velocities are projected onto the profile lines along great circles. Also, rotations produce no normal strain rates in the velocity field (i.e. dVx/dx = 0 for any orientation of the x-axis in a rotational field), therefore velocities parallel to the profile are not biased and do not change even though some velocity vectors may make significant angles to the profiles.

Strain Rates

Normal strain rates were calculated using weighted, least-squares linear regressions and the velocities listed in Table S-1. Each table lists velocities that corresponds to the Profiles, A, B, C, and D shown in Figure 4 of the manuscript. The equation fit is:

$$V_x = \varepsilon_{xx}\, x + b$$

Where ε_{xx} is the normal strain rate, x is the distance along the profile, Vx is the velocity component in the direction of the profile, and b is the intercept (velocity at the start of the profile).

The weight for each datum is the inverse of its variance. Uncertainties in the strain rates are taken from the covariance matrix.

Table S-1. Horizontal GPS velocities used to calculate strain rates for Profiles A, B, C, and D in Fig. 4.

GPS Site	Distance - x (km)	Velocity - Vx (mm/yr)	Sigma (mm/yr)	Calculated Velocity (mm/yr)
ε_{xx}= 7.3 ± 0.4 x 10^{-9}yr^{-1} from 160 to 517 km (Profile A, Centennial Tectonic Belt)				
HLID	160.31	-2.30	0.20	-2.59
OBSN	167.15	-2.23	0.24	-2.54
008A	170.09	-3.10	0.35	-2.52
WODI	176.15	-2.50	0.54	-2.48
S014	180.51	-2.57	0.33	-2.45
Z425	217.72	-2.81	0.24	-2.18
TCSG	224.18	-2.51	0.23	-2.13
P354	225.07	-2.01	0.30	-2.12
ANDF	228.24	-2.04	0.32	-2.10
CRAW	231.48	-2.12	0.41	-2.08
CIND	232.71	-2.33	0.44	-2.07
R015	233.14	-1.74	0.36	-2.06
X51X	239.58	-1.54	0.43	-2.02
DARI	241.06	-2.48	0.40	-2.01
DONP	254.37	-1.14	0.36	-1.91
HPIG	254.85	-2.61	0.26	-1.91
DONK	262.37	-1.55	0.23	-1.85
P679	263.38	-2.24	0.56	-1.84
C054	268.75	-1.98	0.35	-1.81
BCYI	275.48	-1.55	0.20	-1.76
EMIG	290.00	-1.75	0.26	-1.65
BIRC	293.34	-1.80	0.35	-1.63

Table S-1. Continued.

GPS Site	Distance - *x* (km)	Velocity - *Vx* (mm/yr)	Sigma (mm/yr)	Calculated Velocity (mm/yr)
A038	297.33	-1.67	0.38	-1.60
GILM	297.95	-1.14	0.32	-1.59
LEAD	302.02	-1.08	0.23	-1.56
ICIG	306.11	-1.63	0.44	-1.53
CABI	328.34	-1.50	0.41	-1.37
P681	330.24	-1.59	0.61	-1.36
G318	346.95	-1.10	0.69	-1.24
SGCK	365.38	-0.69	0.59	-1.10
P706	379.94	-0.70	0.31	-1.00
PRIC	381.47	-1.52	0.68	-0.99
DILL	386.64	-1.30	0.21	-0.95
SWET	397.81	-0.56	0.66	-0.87
P719	438.07	-0.42	0.31	-0.58
H146	446.02	-0.23	0.25	-0.52
F145	469.39	-0.47	0.25	-0.35
NOMT	472.86	-0.73	0.20	-0.32
G103	475.80	0.36	0.38	-0.30
SQUA	492.15	-0.26	0.61	-0.18
P461	512.66	0.16	0.30	-0.03
BOZE	514.15	0.05	0.29	-0.02
BASE	516.83	-0.09	0.59	-0.004
ε_{xx}= 13.2 ± 2.3 x 10^{-9}yr^{-1} from 218 to 306 km (Profile A, three NW-trending normal faults)				
Z425	217.72	-2.81	0.24	-2.44
TCSG	224.18	-2.51	0.23	-2.35
P354	225.07	-2.01	0.30	-2.34
ANDF	228.24	-2.04	0.32	-2.30
CRAW	231.48	-2.12	0.41	-2.25
CIND	232.71	-2.33	0.44	-2.24
R015	233.14	-1.74	0.36	-2.23
X51X	239.58	-1.54	0.43	-2.15
DARI	241.06	-2.48	0.40	-2.13
DONP	254.37	-1.14	0.36	-1.95
HPIG	254.85	-2.61	0.26	-1.95
DONK	262.37	-1.55	0.23	-1.85
P679	263.38	-2.24	0.56	-1.83
C054	268.75	-1.98	0.35	-1.76
BCYI	275.48	-1.55	0.20	-1.67
EMIG	290.00	-1.75	0.26	-1.48
BIRC	293.34	-1.80	0.35	-1.44
A038	297.33	-1.67	0.38	-1.39
GILM	297.95	-1.14	0.32	-1.38
LEAD	302.02	-1.08	0.23	-1.32
ICIG	306.11	-1.63	0.44	-1.27
ε_{xx}= -0.4 ± 0.6 x 10^{-9}yr^{-1} from 80 to 403 km (Profile B, Snake River Plain)				
TWFA	79.69	-2.74	0.24	-2.70
H422	91.25	-2.35	0.27	-2.70
SHOG	114.89	-2.57	0.34	-2.71
Y423	133.31	-3.19	0.20	-2.72

Table S-1. Continued.

GPS Site	Distance - *x* (km)	Velocity - *Vx* (mm/yr)	Sigma (mm/yr)	Calculated Velocity (mm/yr)
P677	146.22	-2.90	0.31	-2.73
32FM	186.70	-2.70	0.24	-2.74
GTRG	211.47	-2.64	0.20	-2.75
0Z36	235.38	-2.79	0.34	-2.76
5223	235.75	-2.59	0.22	-2.76
COBB	249.97	-2.74	0.26	-2.77
GRAF	251.80	-2.48	0.36	-2.77
N056	252.06	-2.77	0.28	-2.77
P678	253.44	-2.66	0.30	-2.77
AECU	253.90	-2.76	0.29	-2.77
ABDI	259.93	-3.05	0.26	-2.77
ARNG	279.79	-2.19	0.26	-2.78
BUSH	289.68	-2.85	0.26	-2.79
CIRC	290.05	-2.47	0.20	-2.79
I107	303.25	-2.96	0.20	-2.79
TERI	316.56	-2.73	0.52	-2.80
RGBY	324.51	-2.77	0.25	-2.80
I132	331.46	-2.66	0.26	-2.81
U11D	343.81	-3.66	0.23	-2.81
P685	357.52	-2.97	0.42	-2.82
P684	372.24	-2.84	0.23	-2.82
JNWY	402.86	-2.52	0.30	-2.84
ε_{xx}= 1.3 ± 2.3 x 10^{-9}yr^{-1} from 187 to 290 km (Profile B, four volcanic rift zones)				
32FM	186.70	-2.70	0.24	-2.74
GTRG	211.47	-2.64	0.20	-2.70
0Z36	235.38	-2.79	0.34	-2.67
5223	235.75	-2.59	0.22	-2.67
COBB	249.97	-2.74	0.26	-2.65
GRAF	251.80	-2.48	0.36	-2.65
N056	252.06	-2.77	0.28	-2.65
P678	253.44	-2.66	0.30	-2.65
AECU	253.90	-2.76	0.29	-2.65
ABDI	259.93	-3.05	0.26	-2.64
ARNG	279.79	-2.19	0.26	-2.61
BUSH	289.68	-2.85	0.26	-2.60
CIRC	290.05	-2.47	0.20	-2.60
ε_{xx}= 6.4 ± 0.5 x 10^{-9}yr^{-1} from 10 to 535 km (Profile C, Intermountain Seismic Belt and Great Basin)				
ELKO	9.70	-3.91	0.20	-4.53
H348	155.49	-3.11	0.64	-3.59
F381	186.09	-3.36	0.62	-3.40
X95X	228.28	-3.11	0.49	-3.12
P100	245.23	-3.46	0.33	-3.01
P111	264.57	-3.37	0.27	-2.89
NGRI	281.80	-3.34	0.30	-2.78
P121	287.56	-3.10	0.20	-2.74
P057	291.05	-2.74	0.22	-2.72
P675	305.14	-2.95	0.31	-2.63

Table S-1. Continued.

GPS Site	Distance - *x* (km)	Velocity - *Vx* (mm/yr)	Sigma (mm/yr)	Calculated Velocity (mm/yr)
DRUF	334.98	-2.32	0.34	-2.44
I762	364.76	-2.89	0.32	-2.25
BATI	371.06	-2.47	0.31	-2.21
GRCE	390.10	-2.42	0.58	-2.08
GRA5	432.96	-2.48	0.57	-1.81
AHID	454.82	-1.38	0.24	-1.67
W067	461.62	-1.24	0.27	-1.62
ETNA	471.00	-1.59	0.61	-1.56
MASN	507.26	-1.03	0.34	-1.33
U044	535.25	-0.40	0.25	-1.15
ε_{xx}= -2.3 ± 0.5 x 10^{-9}yr^{-1} from 3 to 552 km (Profile D, Oregon and Western Snake River Plain)				
PRIN	3.01	-1.70	0.59	-1.48
BROT	34.85	-1.80	0.36	-1.55
J090	86.06	-1.58	0.37	-1.66
TOMB	161.06	-2.19	0.46	-1.83
D706	162.27	-1.54	0.33	-1.83
P392	169.68	-2.22	0.42	-1.85
GENT	234.68	-2.06	0.25	-2.00
PSTP	264.07	-1.35	0.37	-2.06
N417	319.91	-1.56	0.28	-2.19
S67A	360.83	-1.90	0.25	-2.28
IDT1	382.07	-2.61	0.47	-2.33
E072	383.71	-2.50	0.24	-2.33
PITT	395.94	-2.43	0.35	-2.36
P84R	402.22	-2.68	0.25	-2.37
S418	434.55	-2.60	0.22	-2.45
U76A	435.68	-2.68	0.21	-2.45
V162	438.69	-2.64	0.24	-2.46
KT05	446.41	-2.89	0.44	-2.47
P019	463.55	-2.66	0.38	-2.51
HIL5	470.61	-1.83	0.35	-2.53
P350	491.56	-2.22	0.61	-2.58
M413	506.20	-2.64	0.25	-2.61
SHAM	519.29	-2.76	0.24	-2.64
SHOG	544.66	-2.65	0.34	-2.70
H422	551.68	-2.40	0.26	-2.71

Slip Rates

Slip rates for right-lateral shear were calculated by computing weighted averages of horizontal GPS velocities along Profiles E, F, G, and H shown in Figure 5 of the manuscript. For each profile, the weighted average velocity was computed for GPS sites on the northwest side of the right-lateral shear zone. One weighted average velocity was computed for all GPS sites in the Snake River Plain and was then used in the calculations of slip rates for all profiles. The slip rate was calculated by taking the difference of the weighted average velocities between the GPS sites northwest of the right-lateral shear zone and the Snake River Plain (Table S-2). The slip rate uncertainties were calculated by taking the square root of the sum of the squared errors.

Table S-2. Horizontal GPS velocities and sigmas used to calculate weighted average velocities and errors along Profiles E, F, G, and H (Fig.5).

GPS Site	Velocity (mm/yr)	Sigma (mm/yr)	Velocity/Sigma^2	1/Sigma^2
Slip Rate = 1.8 ± 0.1 mm/yr for Profile E (Centennial fault)				
WSSB	-1.05	0.28	-13.66	13.03
L070	-0.80	0.42	-4.48	5.62
BUTT	-1.05	0.42	-5.91	5.62
DILL	-1.30	0.21	-30.36	23.34
P706	-0.63	0.31	-6.71	10.61
SWET	-0.64	0.66	-1.46	2.28
SGCK	-0.72	0.59	-2.05	2.85
PRIC	-1.54	0.68	-3.39	2.19
G318	-1.13	0.69	-2.42	2.13
Weighted Average	-1.04*	0.12**		
Slip Rate = 1.4 ± 0.1 mm/yr for Profile F (Beaverhead fault)				
SMNA	-1.10	0.28	-13.98	12.76
LEAD	-1.06	0.30	-11.96	11.34
GILM	-1.13	0.24	-19.33	17.08
BCYI	-1.57	0.32	-15.27	9.70
CABI	-1.51	0.35	-12.56	8.31
ICIG	-1.65	0.20	-41.33	25.00
P681	-1.53	0.54	-5.29	3.47
A038	-1.69	0.38	-12.02	7.11
Weighted Average	-1.39*	0.10**		
Slip Rate = 1.1 ± 0.1 mm/yr for Profile G (Lost River fault)				
U15A	-1.76	0.60	-4.86	2.76
ANDF	-2.11	0.32	-20.60	9.77
R015	-1.82	0.36	-14.06	7.72
X51X	-1.63	0.42	-9.13	5.59
P354	-2.06	0.31	-22.12	10.75
DONK	-1.62	0.23	-32.08	19.75
DONP	-1.28	0.36	-10.12	7.93
Weighted Average	-1.76*	0.12**		

Table S-2. Continued.

GPS Site	Velocity (mm/yr)	Sigma (mm/yr)	Velocity/Sigma^2	1/Sigma^2
Slip Rate = 0.7 ± 0.2 mm/yr for Profile H (Sawtooth fault)				
LOMN	-1.86	0.30	-21.13	11.34
OBSN	-2.32	0.24	-39.58	17.08
Weighted Average	-2.14*	0.19**		
Snake River Plain (GPS sites from all profiles)				
GRAF	-2.52	0.36	-19.44	7.72
0Z36	-2.87	0.34	-24.80	8.65
5223	-2.66	0.22	-53.97	20.29
32FM	-2.79	0.24	-50.52	18.11
AECU	-2.80	0.29	-33.29	11.89
COBB	-2.80	0.26	-41.46	14.79
GTRG	-2.72	0.20	-67.95	25.00
RM55	-2.89	0.33	-27.35	9.47
I585	-2.84	0.38	-19.43	6.85
CIRC	-2.49	0.20	-62.18	25.00
TERI	-2.69	0.52	-9.96	3.70
ARNG	-2.22	0.26	-33.63	15.14
P678	-2.67	0.31	-28.73	10.75
BUSH	-2.84	0.26	-41.95	14.79
N056	-2.82	0.28	-35.98	12.76
I107	-3.00	0.20	-74.90	25.00
ABDI	-3.10	0.26	-45.80	14.79
I762	-2.90	0.32	-28.83	9.95
I132	-2.62	0.26	-39.71	15.14
P685	-2.92	0.42	-16.82	5.75
U11D	-3.70	0.24	-64.17	17.36
P684	-2.80	0.23	-51.17	18.26
RGBY	-2.78	0.25	-43.71	15.75
JNWY	-2.48	0.31	-26.11	10.54
U59A	-3.14	0.23	-60.31	19.24
SHAM	-2.71	0.25	-45.10	16.66
SHOG	-2.71	0.34	-23.47	8.65
P677	-3.00	0.31	-31.84	10.61
H422	-2.47	0.27	-34.69	14.03
Y423	-3.32	0.20	-83.10	25.00
Weighted Ave	-2.83*	0.05**		

* - Weighted average velocity was computed by dividing the sum of velocity/sigma^2 by the sum of 1/sigma^2.

** - Error calculated by taking one over the square-root of the sum of 1/sigma^2.

Earthquake Slip Vectors from Focal mechanisms

Focal mechanisms shown in Fig. 1 of the manuscript were compiled from: Zollweg & Richins (1985); Richins *et al.* (1987); Jackson & Zollweg (1988); Doser & Smith (1989); Jackson *et al*. (1993); Pezzopane & Weldon (1993); Stickney (1997; 2007); http://www.seismology.harvard.edu/; and http://www.eas.slu.edu/Earthquake_Center/MECH.NA/index.html. Slip vectors used in the inversions are listed in Table S-3 and shown in Fig. S-1. We also list the slip vectors predicted for the preferred model ctb9 (also shown in Fig. 9 of the manuscript).

Table S-3. Slip vectors of earthquakes used in the inversions and predicted slip vector from preferred model ctb9.

	Event	Epicenter			Fault Plane Solution[b]				Model ctb9	
ID	(Year, Month, Day, Hour, and Minute)	Longitude (°W)	Latitude (°N)	**M**[a]	Strike (°)	Dip (°)	Rake (°)	Slip Vector (°N)	Predicted Slip Vector (°N)	Reference
1	1915 10 03 06:52	-117.50	40.50	6.9	194	44	-61	104	120	1
2	1916 02 03 05:03	-117.80	41.00	6.5	194	44	-61	246	331	1
3	1925 06 27 01:21	-111.33	46.08	6.6	250	56	-38	274	nc	2
4	1962 08 30 13:35	-111.60	41.92	5.9	201	49	-108	315	277	2
5	1982 11 04 09:58	-111.81	44.71	3.6[a]	54	72	-157	227	222	3
6	1986 09 26 22:48[c]	-114.66	44.00	4.5[a]	140	55	-110	50	nc	4
7	1994 02 03 09:05	-111.14	42.73	5.8	4	40	-79	274	265	5
8	1995 01 28 06:26	-114.83	44.51	4.3	160	76	-47	70	88	6
9	2001 04 21 17:18	-111.29	43.02	5.1	349	47	-105	259	267	6
10	2005 07 26 04:08	-112.61	45.35	5.5	359	58	-42	269	nc	6, 7
11	2006 06 18 00:05	-111.90	45.60	4.2	305	60	-120	215	nc	6, 7
12	2007 05 08 15:46	-112.13	45.39	4.4	345	55	-85	255	nc	6, 7
13	2010 08 05 00:04	-110.44	43.58	4.8	45	75	-25	52	35	6
14	2011 04 05 07:05	-112.10	44.62	4.6	36	74	-157	210	222	5

nc – Not calculated in ctb9 model since the fault plane solution is near a block boundary that was not included in the model.

a. Moment magnitude unless otherwise indicated. The 1982 (3.6) and 1986 (4.5) are local magnitudes (M_L).

b. Measured positive clockwise from north and for right-hand rule.

c. Focal mechanism is representative of more than 30 events within the swarm associated with the largest magnitude event listed.

References: (1) Pezzopane & Weldon (1993); (2) Doser & Smith (1989); (3) Stickney (1997); (4) Jackson & Zollweg (1988); (5) http://www.globalcmt.org/CMTsearch.html/; (6) http://www.eas.slu.edu/Earthquake_Center/MECH.NA/index.html; (7) Stickney (1997; 2007).

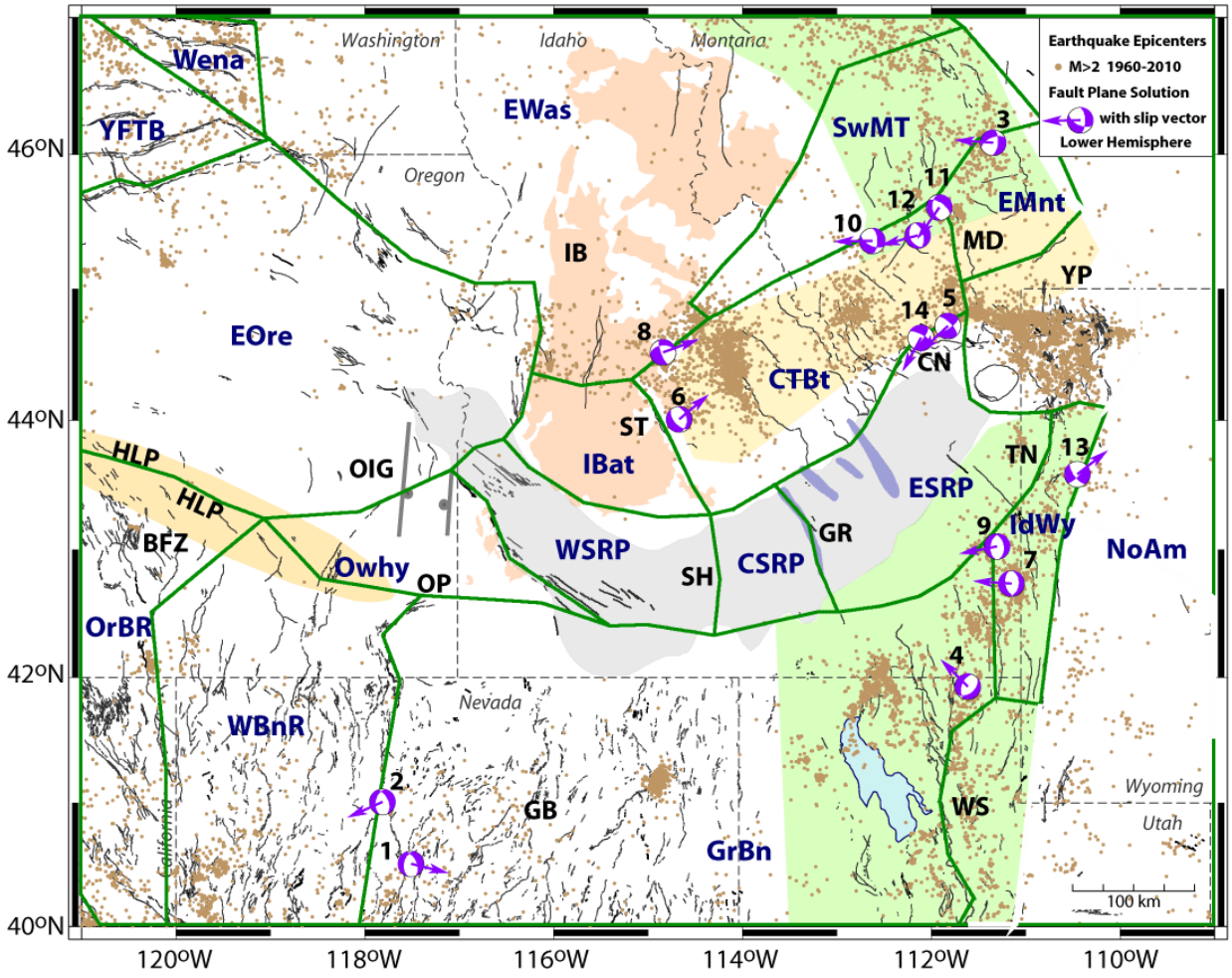

Figure S-1. Map shows locations of focal mechanisms with slip vectors and identification numbers that correspond to Table S-3. Green lines show block boundaries with block names (blue letters) for all blocks. The block model shown is not specific to any model, Figures S-2 to S-9 show models used in the inversions. Shaded tectonic provinces and geologic features: Centennial Tectonic Belt (yellow); HLP – High Lava Plains (orange); IB – Idaho Batholith (salmon); Intermountain Seismic Belt (green); ESRP – Eastern Snake River Plain, CSRP – Central Snake River Plain, and WSRP – Western Snake River Plain (gray); BFZ – Brothers Fault Zone; GB – Great Basin; OIG – Oregon-Idaho Graben; OP – Owyhee-Oregon Plateau; YP – Yellowstone Plateau. Quaternary faults from: http://earthquake.usgs.gov/regional/qfaults/ and Holocene normal faults labeled for CN – Centennial; MD – Madison; ST – Sawtooth; TN – Teton; and WS – Wasatch. Volcanic rift zones (blue-gray) and the Holocene Great Rift is labeled GR and Shoshone, SH. Earthquake epicenters (brown dots) compiled for magnitudes greater than 2.0 from 1960 to 2010 (http://www.ncedc.org/anss/catalog-search.html).

Calculation of Dike Opening Rates

We use horizontal displacements and ages of lava flows presented by Holmes *et al*. (2008) for the Great Rift to estimate dike-opening rates. In the inversions for models max1, max2, and max3, we use the range from 0.16 to 2.03 mm/yr for minimum and maximum rates, respectively (Table S-5). TDEFNODE solves for the dike opening rates within this range that is supported by the data to minimize the χ_n^2 of the misfit to the weighted data.

Table S-5. Dike-opening rates calculated for the Great Rift volcanic rift zone.

Time (yr)	Horizontal Displacement		Estimated Rate		Description
	Minimum (mm)	Maximum (mm)	Minimum (mm/yr)	Maximum (mm/yr)	
4,500	740	1570	0.16	0.35	Estimated dike opening rates based on amount of extension measured across the 4-km long Minidoka cracks and the estimated minimum eruptive time period from crosscutting relationships of dated lava flows (Holmes *et al*. 2008).
2,222	760	4500	0.34	2.03	Estimated dike opening rates based on amount of extension measured across the 14-km long Kings Bowl cracks and the estimated minimum eruptive time period from the age of the Kings Bowl lava flow (Kuntz *et al*. 1992; Holmes *et al*. 2008).
4,500	1330	4410	0.30	0.98	Estimated dike opening rates based on amount of extension measured across the 14-km long New Butte cracks and the estimated eruptive time period from ages of associated lava flows (Kuntz *et al*. 1992; Holmes *et al*. 2008).
4,500	6000	8000	0.44	1.78	Estimated dike opening rate based on modeling of crustal extension at depth and the estimated eruptive time period used by Holmes *et al*. (2008) to calculate a maximum regional strain rate.

Selection of Block Model Boundaries

We develop a block model of the Northern Basin and Range Province to test a range of possibilities for deformation in the Snake River Plain and adjacent Basin and Range regions. Boundaries separate tectonic provinces based on knowledge of geology, seismicity, volcanism, active tectonic faults, and regions with observed differences in surface velocities. Here we discuss the basis for selecting the block boundaries for Figure 6 of the manuscript.

Snake River Plain Blocks

We constructed a block model for the Snake River Plain to test the location and kinematics of its boundaries with adjacent tectonic provinces and whether or not volcanic rift zones contribute to its internal deformation. The Snake River Plain is a prominent physiographic feature in the western U.S. and its boundaries are defined by a pronounced change from the topographically low, seismically-quiet, volcanic-dominated province to the higher mountainous terrain of the seismically active surrounding Basin and Range province (e.g. Pierce & Morgan 1992; Anders *et al.* 1989; Wood and Clemens 2002).

The block perimeter of the Snake River Plain in some places follows and in other places deviates from its physiographic boundaries. For example, the northwestern boundary of the eastern Snake River Plain (ESRP) block is placed along the abrupt topographic contrast (Fig. 6a of the manuscript), which also corresponds to the observed step in velocities along Profiles F, G, and H (Fig. 5 of the manuscript). Farther east, this same boundary extends north to include two velocities near the Centennial fault in the ESRP block, which have larger magnitudes than velocities farther to the north in the Centennial Tectonic Belt (CTBt) block (Fig. 6). At this location, the boundary coincides with the step in velocities observed along Profile E (Fig. 5), generally follows the W-trending Holocene Centennial normal fault, and has nearby earthquakes with strike-slip focal mechanisms (Fig. 6a). We also place the ESRP block's southeastern boundary beyond its physiographic boundary to include four velocities that are more similar to those in the Snake River Plain than those in the adjacent Idaho-Wyoming border (IdWy) block within the Intermountain Seismic Belt (Fig. 6b). Boundaries of the western Snake River Plain (WSRP) block generally follow the western Snake River Plain's physiographic boundaries and boundaries of Wood and Clemens (2002) with the exception of its northwestern end, where the boundary is located southeast of its physiographic boundary since there is a reduction in the magnitudes of velocities here (Fig. 6b). Although not part of the Snake River Plain, the Owyhee-Oregon Plateau (Owhy) block has velocities more similar to those in the WSRP block than those to the south in the western Basin and Range (WBnR) block (Fig. 6b). The Owhy block shares its eastern boundary with the WSRP block.

We also separate the Snake River Plain into three blocks (ESRP, CSRP, and WSRP) using two boundaries that represent volcanic rift zones (Fig. 6a). The ESRP block is separated from the CSRP block by a boundary placed along the Great Rift, an 85-km long Holocene volcanic rift zone with eight mafic dike-fed episodes over the last 2,000 to 15,000 yrs (Kuntz *et al.* 1986; 2002; 2007). The WSRP block is separated from CSRP block based on the more westward oriented azimuths of velocities than the southwest oriented azimuths in the CSRP and ESRP blocks. The N-S oriented boundary between the WSRP and CSRP is somewhat east of Wood & Clemens (2002) eastern boundary and is near source vents of the Shoshone volcanic field that has Quaternary basalt flows as young as ~10,000 yrs (Kuntz *et al.* 1986).

Basin and Range and Other Blocks

Around the Snake River Plain, we separate several recognized tectonic provinces and assess the significance of including these boundaries (Fig. 6). North of the Snake River Plain, we add boundaries to create three blocks associated with the Centennial Tectonic Belt and northern part of the Intermountain Seismic Belt (Fig. 6) based largely on differences in the velocities: 1) CTBt, 2) southwest Montana (SwMT), and 3) eastern Montana (EMnt) (meaning easternmost extent of Basin and Range faults). We

place two boundaries along active tectonic faults. The boundary between the EMnt and CTBt blocks is along the N-trending Holocene Madison normal fault (Fig. 6a). Farther west, we separate the CTBt block from the Idaho batholith (IBat) along the NW-trending Holocene Sawtooth normal fault (Thackray *et al.* 2009). We also divide the Idaho batholith into two blocks along the southern edge of a W-trending zone of diffuse seismicity (Fig. 6a) and to include a region with more uniform magnitude velocities in the southern part of the batholith. The western boundary of the IBat block marks a decrease in the magnitudes of velocities similar to that observed along the western end of the western Snake River Plain (Fig. 6b). Since we lack velocities northwest of the IBat and SwMT blocks, we create the eastern Washington (EWas) block, a large block similar to that of McCaffrey *et al.* (2007) that also includes the northern part of the Idaho batholith.

To the west and south of the Snake River Plain, we include a block for eastern Oregon and two for the Great Basin based on McCaffrey (2005) (Fig. 6). The eastern boundary of the Great Basin (GrBn) block coincides with the N-trending Holocene Wasatch normal fault in Utah and its northern end in Idaho extends northward to the Snake River Plain separating velocities with different magnitudes (faster to the west in the GrBn block and slower to the east in the IdWy block; Fig. 6b). A boundary was placed between the WBnR and GrBn blocks based on changes in azimuth from west to northwest oriented velocities (Fig. 6b). For the eastern Oregon (EOre) block, the northern boundary is along the Olympic Wallowa Lineament and the southern boundary is along the Brothers fault zone and High Lava Plains (Fig. 6a). Although we show the westernmost blocks (OrBR, YFTB, and Wena) from McCaffrey *et al.* (2007) in Fig. 6b, we did not include these blocks in the inversions. Velocities in these three blocks are affected by elastic strain of the Cascadia subduction zone (McCaffrey *et al.* 2007), which we do not include in this study. We also excluded velocities west of -119°W longitude in the EOre block for this same reason. In their Fig. 10, McCaffrey et al. (2007) plot components of the velocities parallel to the direction of several E-W profiles (from 47° to 42°N). These profiles show that contractional strain (large negative slopes) due to subduction extends over a distance of 300 km to the east of the Cascadia thrust. East of the Cascade arc volcanoes at distances of 400 to 800 km from the Cascadia thrust, the profiles show nearly flat lines suggesting little contribution of contractional strain from the subduction zone to velocities used in our analyses.

East of the Snake River Plain and Great Basin, we set up the IdWy and North America (NoAm) blocks. The velocities within the IdWy block have consistent azimuths and are slightly greater in magnitude than those to the south in the GrBn block and east in the NoAm block (Fig. 6b). The western boundary of the IdWy block is along the N-trending Holocene Teton normal fault (Smith *et al.* 1993; Byrd *et al.* 1994). The eastern boundary of the IdWy block follows the eastern edge of the Intermountain Seismic Belt generally defined by the drop-off in seismicity (Fig. 6a). The NoAm block is used to establish a reference frame for the other blocks, and is fixed relative to Stable North American Reference Frame (SNARF). Note that in later text we use North America as the indicator of SNARF.

The Yellowstone Plateau (YP) covers the region of transient motions due to episodic inflation and deflation events associated with ongoing deformation of the Yellowstone caldera (e.g. Chang *et al.* 2007; 2010). We did not include this region in our block model configuration because we do not model the transient signals. However, previously Payne *et al.* (2009) found that the transient motions within the caldera do not have an observable impact on GPS sites in the Snake River Plain.

Block Models

We present the block models used in the inversions with TDEFNODE (McCaffrey 2009) to determine a preferred model that fits the GPS and earthquake slip vector data. For the inversions presented, we start with all blocks tied together and rotating with the same angular velocity relative to North America. We then add boundaries to determine their statistical significance in separating tectonic provinces. With this approach, model complexity is statistically evaluated as more boundaries and strain rate tensors are included. The preferred model is determined by finding the limits of when boundaries are added but no statistical significance is found. We also assess the statistical significance of including strain rate tensors and constraining slip rates along boundaries that represent volcanic rift zones (i.e. dike opening rates).

We calculated the statistical significance of model pairs. Table S-4 lists results of F-distribution tests between two models. F distributions were calculated using the reduced chi-square (χ_η^2) and degrees of freedom (DOF) for two models. The F distributions give the probability that the first model is different from second or that the first model has a better fit to the data than the second model. We apply the maximum confidence level of ≥99% to indicate one model with added boundaries has a better fit to the data over a second model (Stein & Gordon 1984).

Model Descriptions

Fig. S-2 shows the thirteen blocks that were used in the model tests. Below, we describe the models used in the inversions and the purpose of each test.

- **Model nb11** (χ_η^2=5.01), Fig. S-3a: The model assumes one pole (P010) and that all blocks (EWas/EOre/WBnR/GrBn/IdWy/ESRP/CSRP/WSRP/Owhy/CTBt/SwMT/EMnt/IBat; see Fig. S-2) rotate with the same angular velocity relative to North America. This model tests whether large-scale regional clockwise rotation alone fits the velocity and earthquake data. The systematic trends in the residuals show that this model has a poorest fit to the data (Fig. S-3a).

- **Model nb13** (χ_η^2=3.36), Fig. S-3b: The model assumes two poles of rotation and a strain rate tensor. Pole P010 is for blocks EWas/EOre/ESRP/CSRP/WSRP/Owhy/CTBt/SwMT/EMnt/IBat and P039 for blocks GrBn/WBnR/IdWy. This model tests whether including a strain rate tensor and adding the southern boundary of the Snake River Plain to separate the Great Basin (represented by P039) fits the velocities. Model nb13 has a lower χ_η^2=3.36 than model nb11 (χ_η^2=5.01) indicating a better fit to the data at >99% probability (Table S-4). Although the Great Basin is separated from the tectonic provinces in the northern part of the Northern Basin and Range, it shows systematic trends in the residuals (Fig. S-3b).

- **Model nb16** (χ_η^2=2.08), Fig. S-4a: The model assumes five poles of rotation and one strain rate tensor. Pole P025 is for multiple blocks ESRP/CSRP/WSRP/Owhy/CTBt/SwMT/EMnt/IBat and the other four poles are for individual blocks. This model tests whether including additional boundaries to separate several tectonic regions is a better fit to the data. Three boundaries are included to divide the Great Basin (GrBn, WBnR, and IdWy blocks) and one is included for the northern part of the Northern Basin and Range (Ewas block). Model nb16 has a lower χ_η^2 and a better fit to the data at >99% probability (Table S-4) over model nb13, and has fewer systematic residuals than the previous two models, nb11 (Fig. 3a) and nb13 (Fig. 3b). Model nb16 (Fig. S-4a) shows that the Western Basin and Range (WBnR block) and the Intermountain Seismic Belt region along the Idaho-Wyoming border (IdWy block) are separate from the Great Basin. It also shows systematic trends in the residuals in the region representing multiple blocks ESRP/CSRP/WSRP/Owhy/CTBt/SwMT/ EMnt/IBat (or P025).

- **Model nbr3** (χ_η^2=1.72), Fig. S-4b: The model assumes seven poles and one strain rate tensor. This model builds upon model nb16 with two boundaries added to test if there is a better fit to the data for separating the Snake River Plain – Owyhee-Oregon Plateau (P029), eastern Oregon (EOre), and Centennial Tectonic Belt (P025). Pole P025 is for blocks CTBt/SwMT/EMnt/IBat, P029 is for blocks ESRP/CSRP/ WSRP/Owhy, and the other five poles are for individual blocks representing tectonic provinces. Model nbr3 has a lower χ_η^2=1.72 than model nb16 (χ_η^2=2.08) indicating a better fit to the data at a 98% probability (Table S-4). This model shows that eastern Oregon (EOre block) and the Snake River Plain – Owyhee-Oregon Plateau (ESRP/CSRP/ WSRP/Owhy) regions are separate tectonic provinces. While the Centennial Tectonic Belt (CTBt/SwMT/EMnt/IBat) is separate from the other tectonic provinces, systematic trends in the residuals remain in the combined block region (Fig. S-4b).

- **Model ctb9** (χ_η^2=1.21), Fig. S-5a: This model assumes seven poles and two strain rate tensors. The model includes the same boundaries to separate tectonic provinces as model nbr3 (see description above). Model ctb9 includes a strain rate tensor to test whether there is an improved fit to the data in the Centennial Tectonic Belt (blocks CTBt/SwMT/EMnt/IBat and labeled as P025; Fig. S-5a). Model ctb9 has a lower χ_n^2=1.21 than model nbr3 indicating a better fit to the data at >99% probability (Table S-4). This model shows that the Centennial Tectonic Belt (CTBt/SwMT/EMnt/IBat) region has an extensional strain rate of 5.7×10^{-9} yr^{-1}.

- **Model ctb7** (χ_η^2=1.16), Fig. S-5b: The model assumes eight poles and two strain rate tensors. The model is the same as ctb9 with the exception of changes to the Centennial Tectonic Belt. In this model, a boundary is added to test whether the Idaho batholith (IBat) is separate from the Centennial Tectonic Belt (pole P025 is for three blocks CTBt/SwMT/EMnt). Model ctb7 has a slightly lower χ_η^2=1.16 than model ctb9 (χ_η^2=1.21), so it fits the data better at a 69% probability over model ctb9 (Table S-4). Model ctb7 relative to ctb9 indicates that further separation of the Centennial Tectonic Belt with additional boundaries (between blocks IBat, CTBt, EMnt, and SwMT) is not warranted.

- **Model wsr1** (χ_η^2=1.21), Fig. S-6a: The model assumes eight poles and two strain rate tensors. The model is the same as ctb9 but includes the boundary for the Great Rift volcanic rift zone in the Snake River Plain (pole P029 is for blocks CSRP/WSRP/Owhy). This model tests whether including the Great Rift volcanic rift zone improves the fit to the data. Model wsr1 does not have a significantly better fit to the data than ctb9 since the probability is 50% (Table S-4).

- **Model max1** (χ_η^2=1.23), Fig. S-6b: The model is the same as wsr1, which includes the Great Rift volcanic rift zone in the Snake River Plain. Model max1 tests whether including dike opening along the Great Rift volcanic rift zone improves the fit to the data. In this model, we constrain dike-opening rates to range from 0.16 to 2.03 mm/yr (Table S-5) with directions listed in Table 3 of the manuscript. Model max1 with dike opening has a 60% degraded fit (Table S-4) to the data when compared to model wsr1. The results suggest that a model with dike opening at rates of 0.16 to 0.29 mm/yr along the Great Rift volcanic rift zone is not supported by the data at close to the one-sigma confidence level.

- **Model wsr2** (χ_η^2=1.21), Fig. S-7a: The model assumes eight poles and two strain rate tensors. It is the same as ctb9 but includes a boundary for the Shoshone volcanic rift zone in the Snake River Plain (i.e. pole P029 is for blocks WSRP/Owhy and P024 is for CSRP/ESRP). Model wsr2 tests whether there is an improved fit to the data for including the Shoshone volcanic rift zone. Model wsr2 does not have a significantly better fit to the data than ctb9 since the probability is 51% (Table S-4).

- **Model max2** (χ_η^2=1.23), Fig. S-7b: The model is the same as wsr2, which includes the Shoshone volcanic rift zone in the Snake River Plain. Model max2 tests whether including dike opening along the Shoshone volcanic rift zone improves the fit to the data. In this model, we constrain dike-opening rates to range from 0.16 to 2.03 mm/yr (Table S-5) with directions listed in Table 3 of the manuscript. Model max2 with dike opening has a 62% degraded fit (Table S-4) to the data when compared to model wsr2. The results suggest that a model with dike opening at rates of 0.16 to 0.23 mm/yr along the Shoshone volcanic rift zone is not supported by the data at close to the one-sigma confidence level.

- **Model wsr3** (χ_η^2=1.21), Fig. S-8a: The model assumes nine poles and two strain rate tensors. It is the same as ctb9 but includes two boundaries in the Snake River Plain for the Great Rift and Shoshone volcanic rift zones (i.e. P029 is for WSRP/Owhy). The model tests whether there is an improved fit to the data for including both volcanic rift zones. Model wsr3 does not have a significantly better fit to the data than ctb9 since the probability is 53% (Table S-4). Models wsr1, wsr2, wsr3, and ctb9 relative to each other indicate that separating the Snake River Plain and Owyhee-Oregon Plateau into smaller blocks is not necessary.

- **Model max3** (χ_η^2=1.29), Fig. S-8b: This model is the same as wsr3, which includes both the Great Rift and Shoshone volcanic rift zones in the Snake River Plain. Model max3 tests whether including dike opening along the both volcanic rift zones improves the fit to the data. In this model, we constrain dike-opening rates to range from 0.16 to 2.03 mm/yr (Table S-5) with directions listed in Table 3 of the manuscript. Model max3 has an 81% degraded fit (Table S-4) to the data when compared to model wsr3. The results suggest that a model with dike opening at rates of 0.16 to 0.33 mm/yr along both the Great Rift and Shoshone volcanic rift zones is not supported by the data at over the one-sigma confidence level.

- **Model vrz1** (χ_η^2=1.49), Fig. S-9a: The model is the same as wsr1, which includes the Great Rift volcanic rift zone in the Snake River Plain. Model vrz1 tests the hypothesis that dike intrusion in the Snake River Plain keeps pace with extension in the Centennial Tectonic Belt. In this model we constrain dike-opening rates to range from 0.96 to 1.36 mm/yr, the GPS-derived extension rate ($13.2\pm2.3\times10^{-9}$ yr^{-1} over 88 km; Profile A, Fig. 4 in the manuscript) across three northwest-trending Basin and Range faults in the Centennial Tectonic Belt. We also constrain the direction of dike opening be within the range shown in Table 3 of the manuscript. Model vrz1 results in dike opening rates of 1.02-0.96 mm/yr for a χ_η^2=1.49. Model vrz1 has a 99% degraded fit (Table S-4) to the data when compared to model wsr1 (without dike opening). The results indicate that a model with dike opening at rates similar to the extension rate across the three northwest-trending faults is not supported by the data at over the two-sigma confidence level.

- **Model esa9** (χ_n^2=1.21), Fig. S-9b: The model is the same as ctb9 but allows elastic strain accumulation along the block boundaries. Model esa9 (Fig. S-9b) has a similar χ_η^2 to that for ctb9 (Fig. S-5a) at the 30% confidence level (Table S-4). Fig. S-10 shows locking of <1 mm/yr (blue arrows) for GPS sites near the two N-trending Great Basin (GrBn) boundaries between the western Basin and Range (WBnR) and Idaho-Wyoming border (IdWy) blocks and the W-trending boundary between the EMnt and NoAm blocks. The W-trending boundary is adjacent to the Yellowstone caldera and we do not correct for any transient effects of recent volcanic activity. We also tested the sensitivity of the velocities to fault-locking. We ran the esa9 model with fault locking on all of the block boundaries (ϕ=1; McCaffrey *et al.* 2007) and at depths from 1 to 15 km. We found the χ_η^2 are similar to that for esa9, thus indicating the data are not sensitive to fault locking. The results indicate that there is very little (<1 mm/yr) elastic strain accumulation (or fault-locking) in the velocity field near the Snake River Plain and we cannot resolve locking depths.

Table S-4. Results of F distribution tests for model pairs.

Model	χ_η^2	DOF	P (%)
nb13	3.36	532	100
nb11	5.01	537	
nb16	2.08	529	100
nb13	3.36	532	
nbr3	1.72	532	98
nb16	2.08	529	
ctb9	1.21	522	100
nbr3	1.72	532	
ctb7	1.16	520	69
ctb9	1.21	522	
ctb9	1.21	522	30
esa9	1.21	497	
wsr1	1.21	519	50
ctb9	1.21	522	
wsr2	1.21	519	51
ctb9	1.21	522	
wsr3	1.21	516	53
ctb9	1.21	522	
wsr1	1.21	519	60
max1	1.23	522	
wsr2	1.21	519	62
max2	1.23	522	
wsr3	1.21	516	81
max3	1.29	522	
wsr1	1.21	519	99
vrz1	1.49	522	

χ_η^2 - Reduced Chi-square; DOF – Degrees of Freedom; P – Probability that misfit variances are from different distributions.

Plots of Model Results

Results are shown in Figs. S-3 to S-10 with the following:

- Pole of rotation (brown dot with 70% confidence ellipse) for poles located within the map region
- Name of a pole (brown letters, e.g. P010 or EWas)
- Residual velocities (gray vectors with 70% confidence ellipses) shown for misfits between observed and predicted velocities
- Principal horizontal strain rate axes (pink arrows) and strain rates (pink letters)
- Block model configuration (solid green lines) showing the boundaries used in the inversions
- Model name (e.g. nb11) and inversion results listed as C2/NP/DF, which corresponds to reduced chi-square (CD), number of free parameters (NP), and degrees of freedom (DF)
- Name (red letters) of the block (e.g. EWas) or name of the pole that has multiple blocks with the same angular velocity (e.g. P010)
- Reduced chi-square of GPS velocities (red numbers) in each block or for all blocks with the same pole of rotation
- Abbreviations (red italics letters) for Great Rift (GR) and Shoshone (SH) volcanic rift zones within the Snake River Plain
- For Fig. S-10 only, elastic strain accumulation at GPS sites (blue vectors).

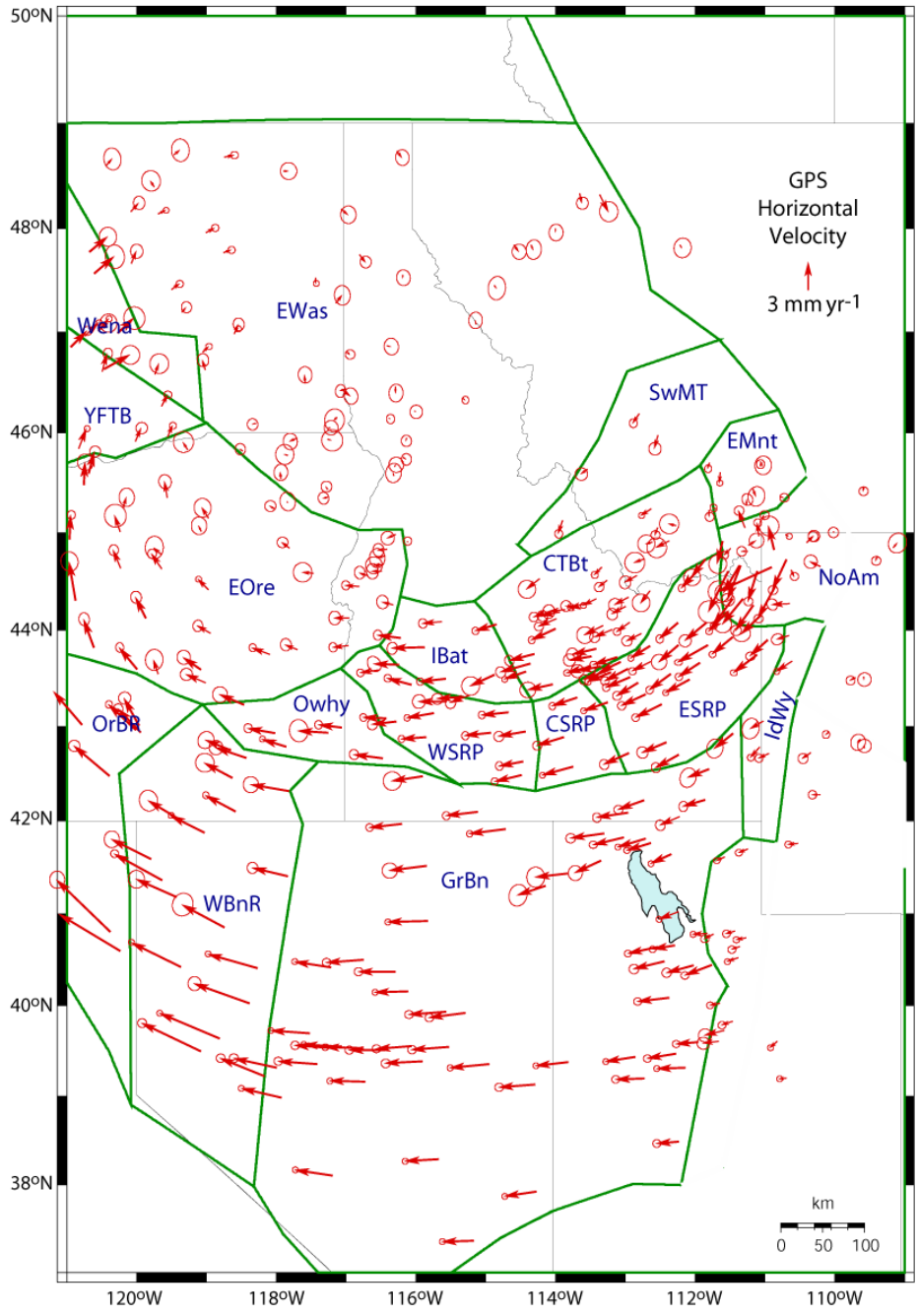

Figure S-2. Map showing the block model (green lines) and horizontal GPS velocities (red vectors with 70% confidence ellipses). The NoAm block is fixed to the Stable North American Reference Frame (SNARF).

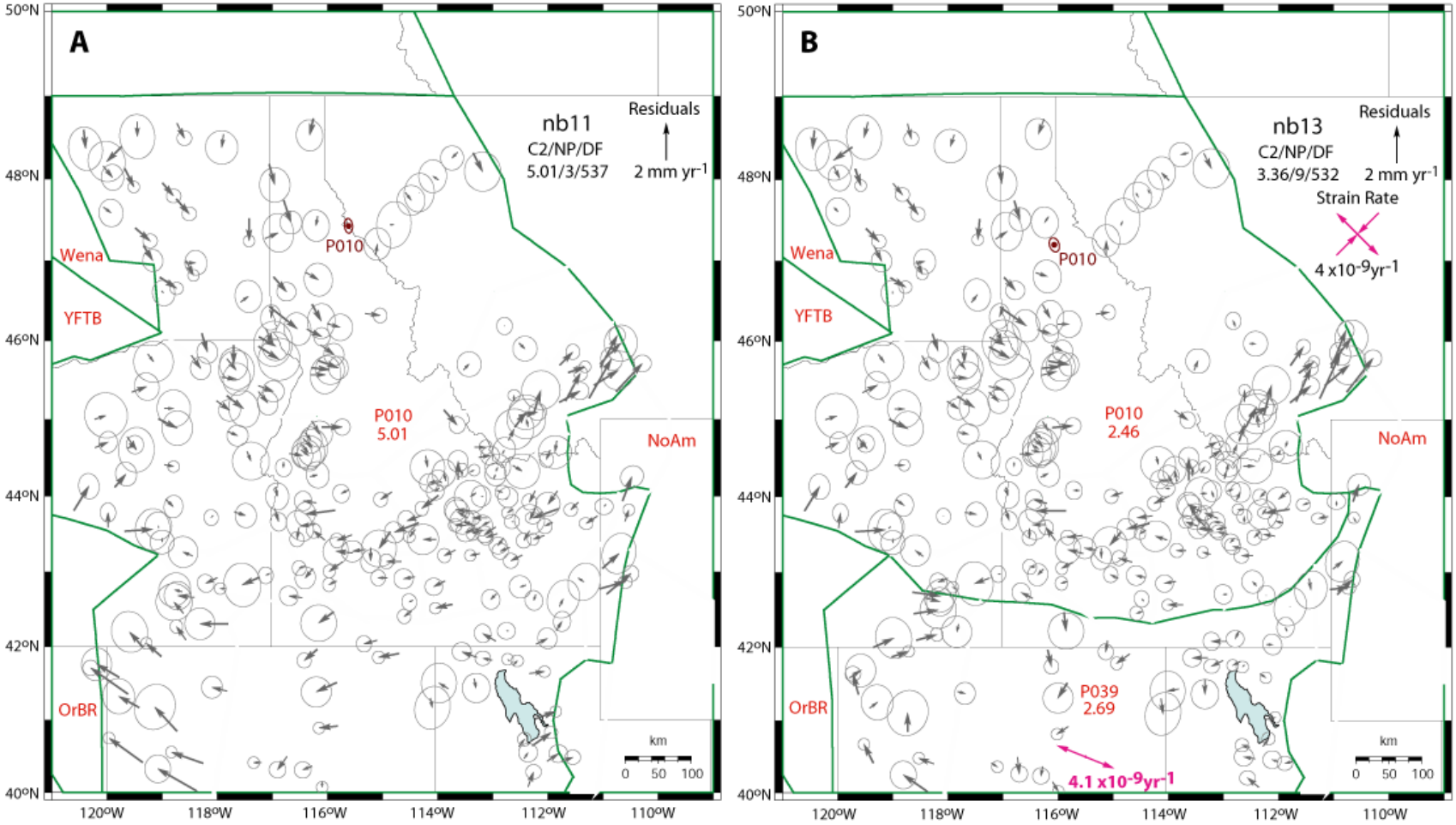

Figure S-3. **nb11**: Model assumes one pole, P010, for all blocks EWas/EOre/WBnR/GrBn/IdWy/ESRP/CSRP/WSRP/Owhy/CTBt/SwMT/EMnt/IBat (see Fig. S-2 for block boundaries). **nb13**: Model assumes two poles, P010 for blocks EWas/EOre/ESRP/CSRP/WSRP/Owhy/CTBt/SwMT/EMnt/IBat and P039 for blocks GrBn/WBnR/IdWy.

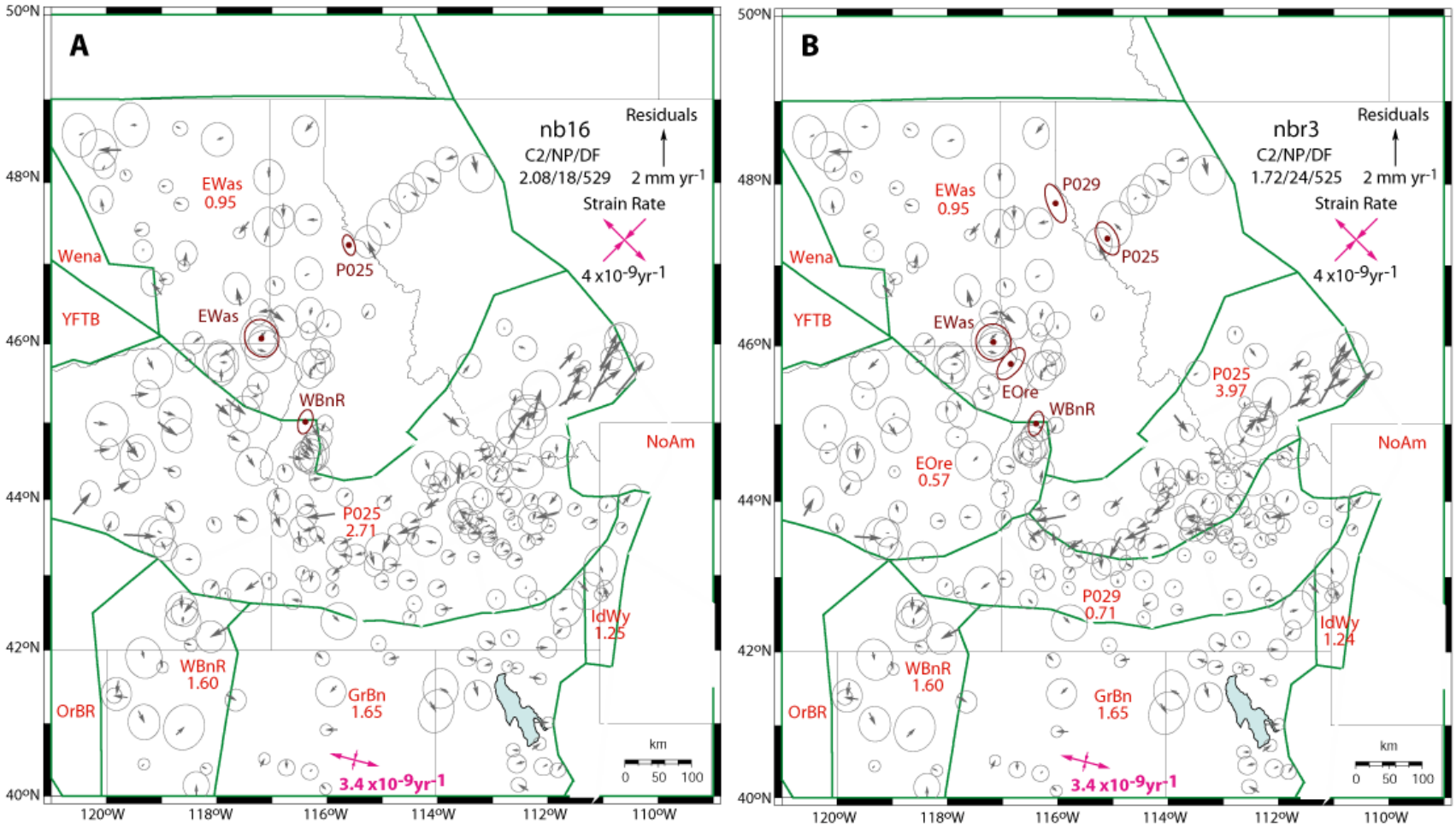

Figure S-4. **nb16**: Model assumes five poles; pole P025 is for multiple blocks ESRP/CSRP/WSRP/Owhy/CTBt/SwMT/EMnt/IBat and all others are individual blocks as labeled. **nbr3**: Model assumes seven poles; pole P025 is for blocks CTBt/SwMT/EMnt/IBat, P029 for blocks ESRP/CSRP/WSRP/Owhy, and all others are individual blocks.

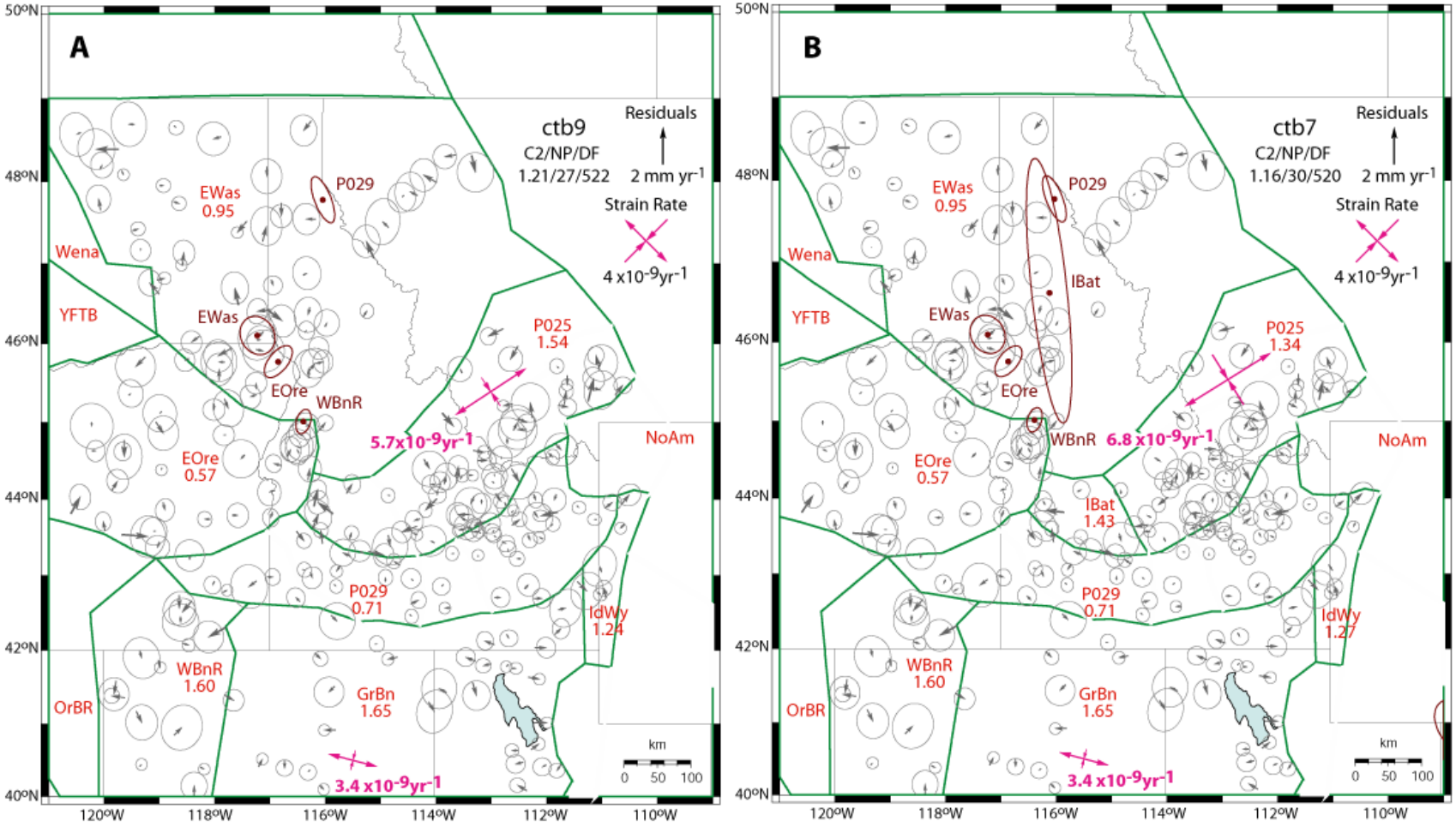

Figure S-5. **ctb9**: Model assumes seven poles; pole P025 is for multiple blocks CTBt/SwMT/EMnt/IBat, P029 for blocks ESRP/CSRP/WSRP/Owhy, and all others are individual blocks as labeled. **ctb7**: Model assumes eight poles; pole P025 is for blocks CTBt/SwMT/EMnt, P029 for blocks ESRP/CSRP/WSRP/Owhy, and all others are individual blocks.

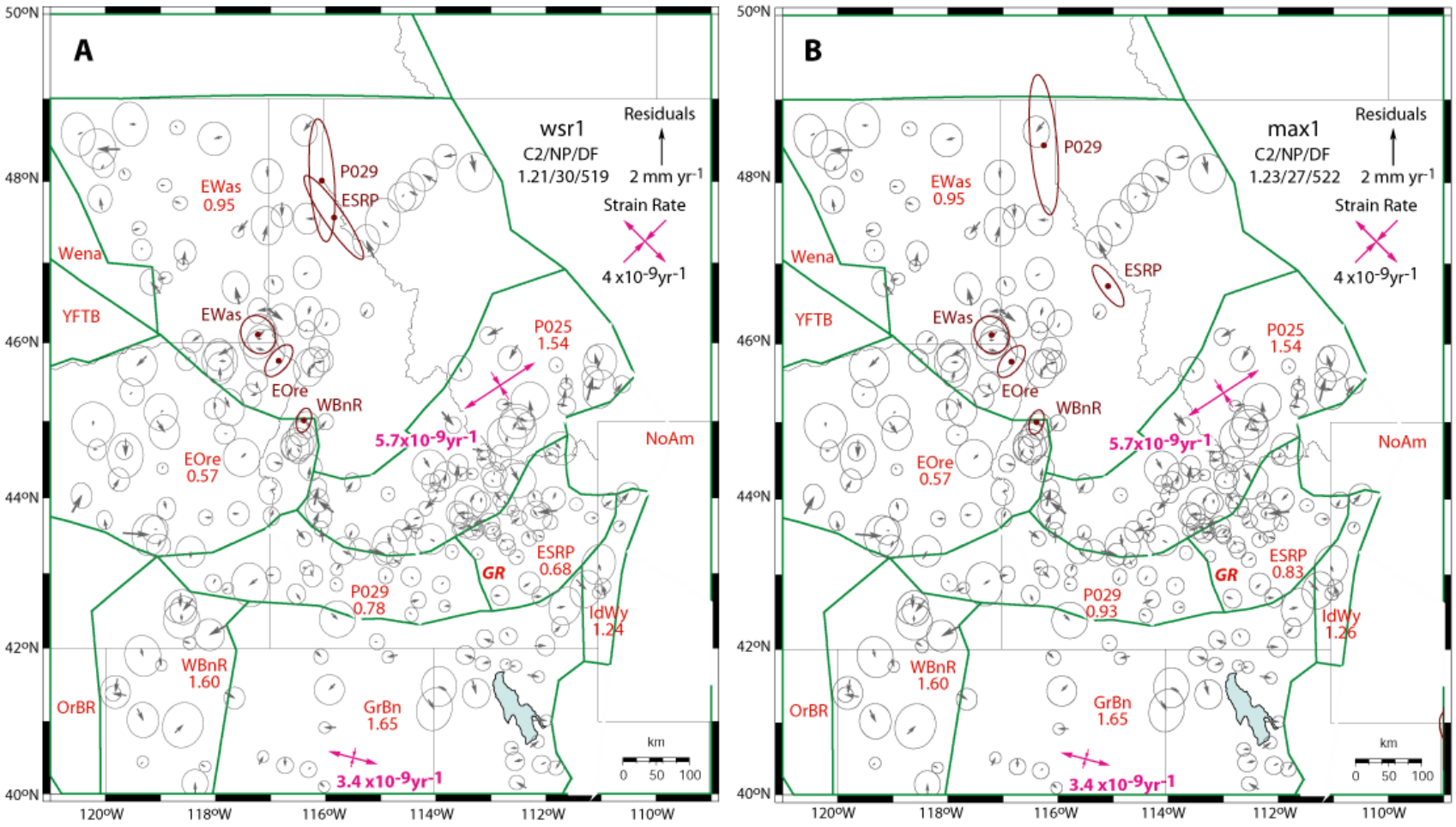

Figure S-6. Models **wsr1** and **max1** assume eight poles; pole P025 is for multiple blocks CTBt/SwMT/EMnt/IBat, P029 for blocks CSRP/WSRP/Owhy, and all others are individual blocks as labeled. Model **max1** forces dike opening along the Great Rift (GR) volcanic rift zone.

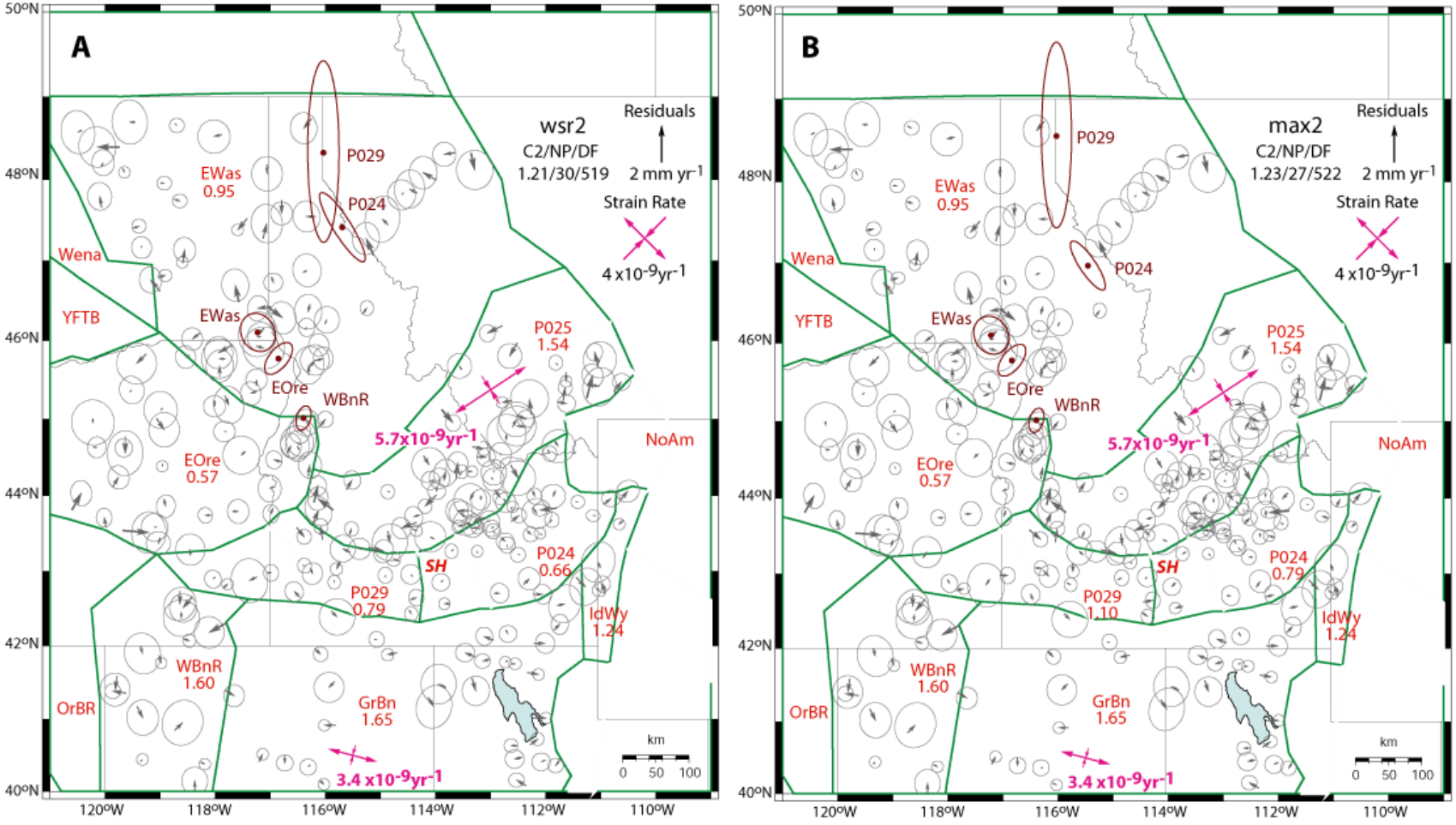

Figure S-7. Models **wsr2** and **max2** assume eight poles; pole P025 is for multiple blocks CTBt/SwMT/EMnt/IBat, P024 for blocks ESRP/CSRP, P029 for blocks WSRP/Owhy, and all others are individual blocks as labeled. Model **max2** forces dike opening along the Shoshone (SH) volcanic rift zone.

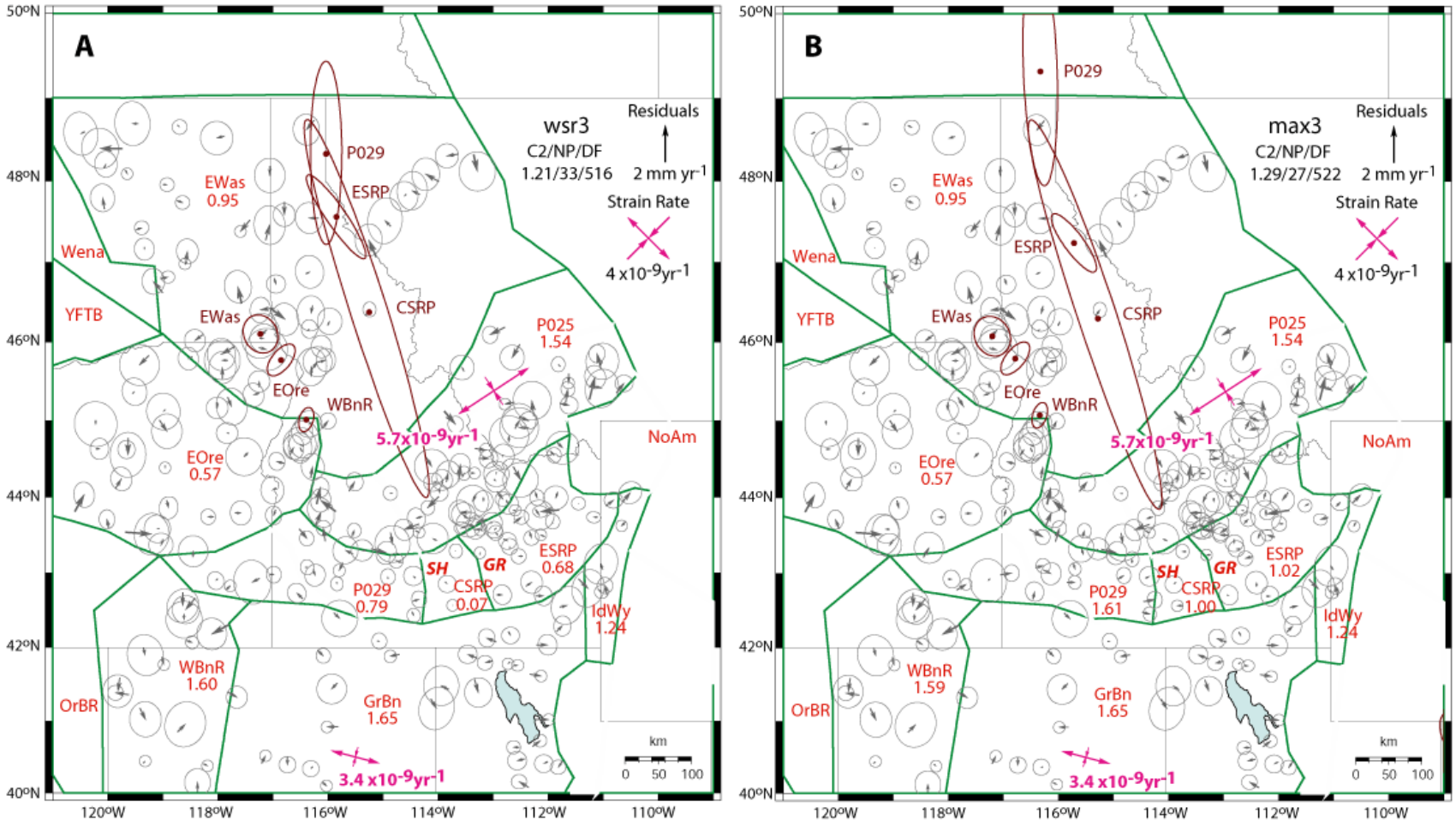

Figure S-8. Models **wsr3** and **max3** assume nine poles; pole P025 is for multiple blocks CTBt/SwMT/EMnt/IBat, P029 for blocks WSRP/Owhy, and all others are individual blocks as labeled. Model **max3** forces dike opening along the Great Rift and Shoshone (SH) volcanic rift zones.

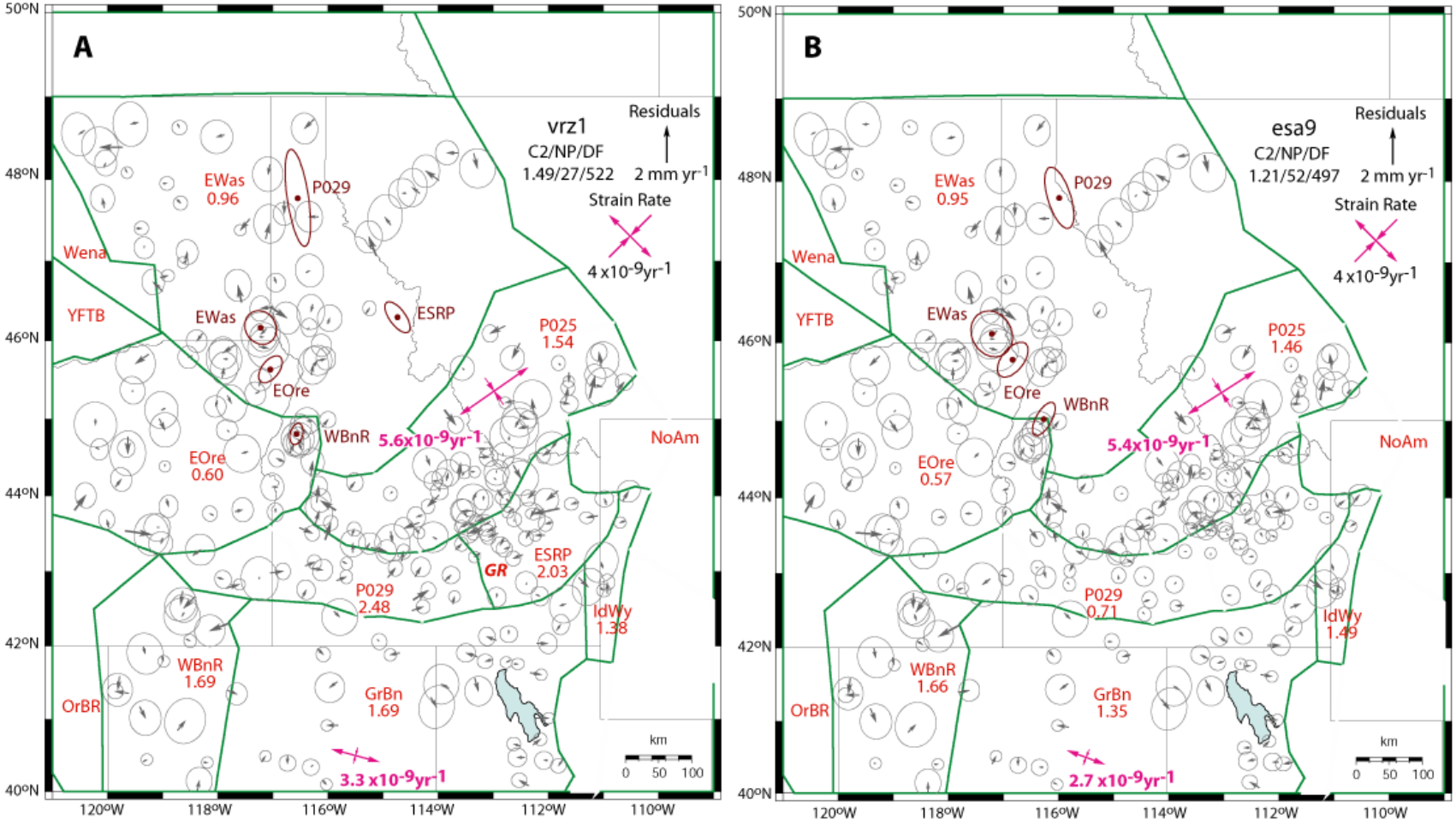

Figure S-9. **vrz1:** Model assumes eight poles; pole P025 is for multiple blocks CTBt/SwMT/EMnt/IBat, P029 for blocks CSRP/WSRP/Owhy, and all others are individual blocks as labeled. Model vrz1 forces dike opening at a rate similar to the extensional rate for three faults in the Centennial Tectonic Belt. **esa9**: Model includes elastic strain accumulation along block boundaries and assumes seven poles (similar to ctb9); pole P025 is for multiple blocks CTBt/SwMT/EMnt/IBat, P029 for blocks ESRP/CSRP/WSRP/Owhy, and all others are individual blocks as labeled.

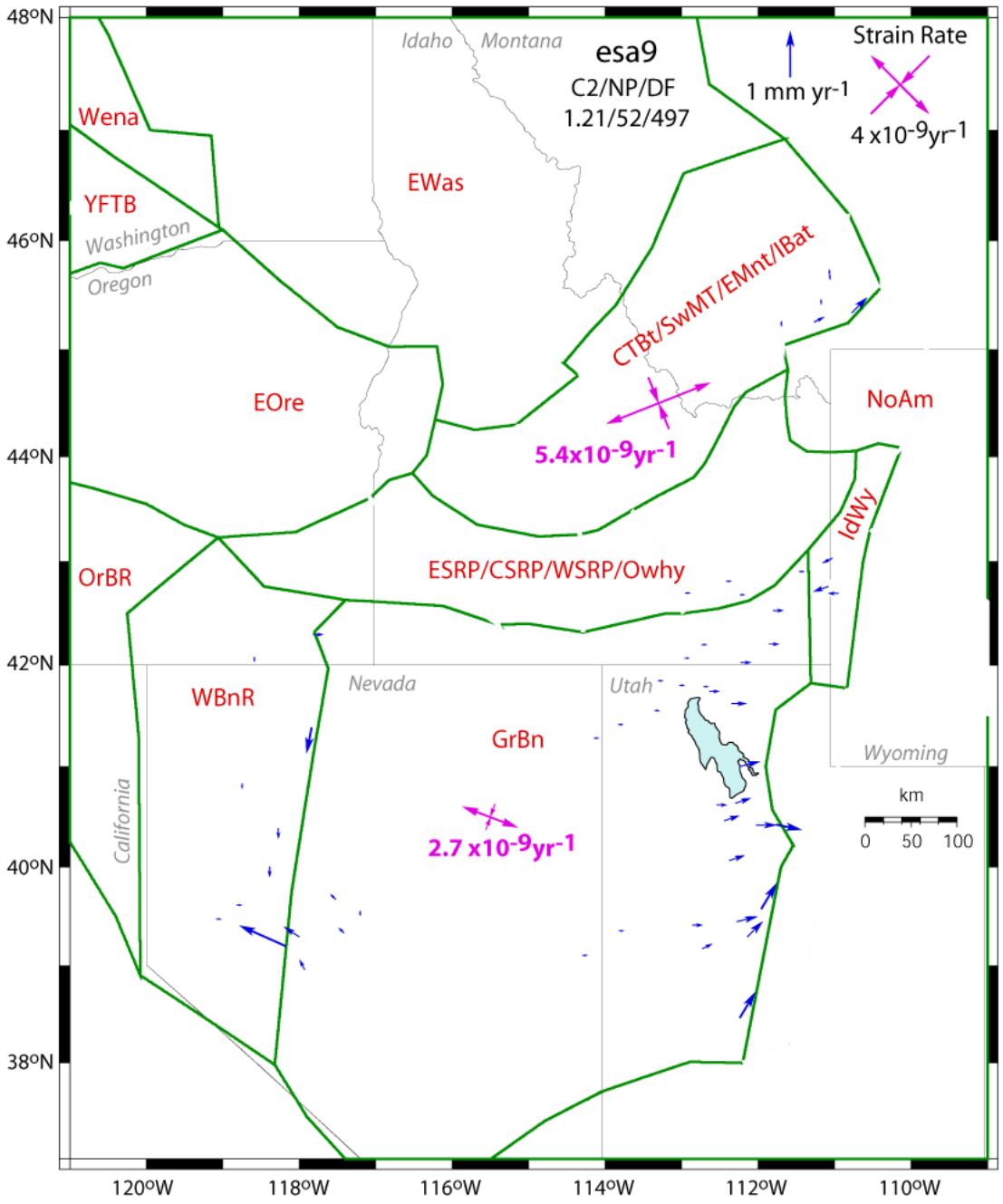

Figure S-10. Inversion results for model eas9 showing GPS sites with elastic strain accumulation.

Post-Seismic Relaxation Evaluation

We evaluate the 1994-2010 velocity field for the presence of post-seismic viscoelastic relaxation signals from the 1983 **M** 6.9 Borah Peak, Idaho and 1959 **M** 7.3 Hebgen Lake, Montana earthquakes. We acquired (Nishimura, Per. Comm. 2010) and used model parameters from Nishimura & Thatcher (2003) along with VISCO1D (Pollitz 1992) to reproduce the synthetic post-seismic horizontal velocity field in 2002 (shown in their Fig. 11). Fig. S-11 shows our synthetic post-seismic velocities from VISCO1D in a grid format for the region surrounding the Snake River Plain. We reproduced the results of Nishimura & Thatcher (2003) for three separate planar slip sources, one for Borah Peak and two for Hebgen Lake, each producing its own predicted velocity field. Their structure is a 40-km-thick elastic crust overlying a mantle viscosity of $4x10^{18}$ Pa-s (see Tables S-6 and S-7 for other parameters). In six different tests, we use the preferred model ctb9 (Fig. S-5a) to evaluate the 1994-2010 velocity field for post seismic signals.

Post-seismic Model Descriptions

The first three models (s1mr, s2mr, and s3mr) test whether the preferred model ctb9 fits the 1994-2010 velocity field after correcting it for post-seismic velocities of Nishimura & Thatcher (2003). Post-seismic velocities were generated using a structure with a 40-km-thick elastic crust overlying a mantle viscosity of $4x10^{18}$ Pa-s and the three earthquake sources (Fig. S-11).

- **Model s1mr** (χ_η^2=1.53), Fig. S-13a: We ran the inversion using preferred model ctb9 with the 1994-2010 velocity field corrected for post-seismic velocities of Nishimura & Thatcher (2003) (Fig. S-12). This test evaluates whether there is an improved fit of the preferred model ctb9 to the velocity field when corrected for post-seismic signals. Results for model s1mr in Fig. S-13a show a >99% (Table S-8) degraded fit with a higher χ_η^2 of 1.53 when compared to model ctb9 with a $\chi_\eta^2$of 1.21 (Fig. S-5a). The results of this test indicate that post-seismic signals generated by Nishimura & Thatcher (2003) are not present in the 1994-2010 velocity field.

- **Model s2mr** (χ_η^2=1.53), Fig. S-13b: We ran another inversion using preferred model ctb9 with the 1994-2010 velocity field corrected for post-seismic velocities of Nishimura & Thatcher (2003) (Fig. S-12). In this model, we also included a strain rate tensor in the Snake River Plain and Owyhee-Oregon Plateau combined region (ESRP/CSRP/ WSRP/Owhy). This model tests whether the low strain rate within the Snake River Plain combined block region is a result of post-seismic relaxation effects. Model s2mr (Fig. S-13b) has a higher χ_η^2 of 1.53 when compared to model ctb9 (χ_η^2=1.21; Fig. S-5a), and a similar result when compared to model s1mr (χ_η^2=1.53) (Fig. S-13a). The results of this test indicate that post-seismic relaxation effects are not the cause of a low strain rate in the Snake River Plain since model s2mr has a >99% probability difference from model ctb9 (Table S-8).

- **Model s3mr** (χ_η^2=1.21), Fig. S-14a: We ran yet another inversion using preferred model ctb9 with the 1994-2010 velocity field corrected for post-seismic velocities of Nishimura & Thatcher (2003) (Fig. S-12). In this inversion, we allowed a scaling factor for each of the three earthquake viscoelastic relaxation velocity fields (Fig. S-12) to adjust as needed to improve the fit of the model to the data. Essentially, we compute a Greens function, then solve for the amplitudes. Fig. S-14a shows a χ_η^2=1.21 for model s3mr, similar to a χ_η^2 of 1.21 for model ctb9 (Fig. S-5a). The χ_η^2 of 1.21 for model s3mr was achieved for values of 0.0 for amplitudes or no changes to the 1994-2010 GPS velocities. The results of this test also indicate that post-seismic signals generated by Nishimura & Thatcher (2003) are not present in the 1994-2010 velocity field.

The last three models (s4mr, s5mr, and s6mr) evaluate the upper bound mantle viscosity that would dampen out the post-seismic signals by 2002.5 (June 2002). Using VISCO1D, we generate three synthetic

post-seismic velocity fields shown in Figures S-15, S-16, and S-17 using three different mantle viscosities: $4x10^{17.5}$, $4x10^{17}$, and $4x10^{16}$ Pa-s, respectively (and keeping other parameters in Tables S-6 and S-7 the same). These viscosities were chosen to evaluate values at and beyond the lower end of the range for $4x10^{18\pm0.5}$ Pa-s estimated by Nishimura & Thatcher (2003). The 1994-2010 velocity field was corrected using the synthetic velocities generated for the three mantle viscosities. We then ran inversions using TDEFNODE with the preferred model ctb9 and the three alternative corrected velocity fields.

- **Model s4mr** (χ_η^2=1.36), Fig. S-14b: This inversion tests whether there is an improved fit of the preferred model ctb9 to the velocity field when corrected for post-seismic velocities generated using a mantle viscosity of $4x10^{17.5}$ Pa-s (low end of Nishimura & Thatcher 2003). Model s4mr (Fig. S-14b) has a degraded fit to the data (higher χ_η^2=1.36) at the 91% probability (Table S-8) when compared to model ctb9 (χ_η^2=1.21, Fig. S-5a). The results of this model indicate post-seismic signals generated by a mantle viscosity of $4x10^{17.5}$ Pa-s (Fig. S-15) are too large and not present in the 1994-2010 velocity field.

- **Model s5mr** (χ_η^2=1.26), Fig. S-18a: The inversion tests whether there is an improved fit of the preferred model ctb9 to the velocity field when corrected for post-seismic velocities generated using a mantle viscosity of $4x10^{17}$ Pa-s. Model s5mr (Fig. S-18a) has a χ_η^2=1.26 indicating a degraded fit to the data at a 70% probability (Table S-8) over model ctb9 (χ_η^2=1.21, Fig. S-5a). Although the post-seismic signals generated by a mantle viscosity of $4x10^{17}$ Pa-s (Fig. S-16) are lower than those for a mantle viscosity used in s4mr, they are still not observed in the 1994-2010 velocity field. This result implies that the actual post-seismic signals from the 1959 and 1983 earthquakes have been dampened out by 2002.

- **Model s6mr** (χ_η^2=1.25), Fig. S-18b: This inversion tests whether there is an improved fit of the preferred model ctb9 to the velocity field when corrected for post-seismic velocities generated using a mantle viscosity of $4x10^{16}$ Pa-s. Model s6mr (Fig. S-18b) has a higher χ_η^2=1.25 and a degraded fit to the data at a 67% probability (Table S-8) over model ctb9 (χ_η^2=1.21, Fig. S-5a). These results are similar to those for s5mr. The much lower velocities generated by a mantle viscosity of $4x10^{16}$ Pa-s (Fig. S-17) are still not observed in the 1994-2010 velocity field. These results further support the implication that the actual post-seismic signals from the 1959 and 1983 earthquakes have been dampened out by 2002.

Table S-6. Input parameters to VISCO1D from Nishimura & Thatcher (2003) for earthquake sources.

Earthquake Sources	1983 Borah Peak (BP1)	1959 Hebgen Lake (HL1)	1959 Hebgen Lake (HL2)
Date	1983.82	1959.63	1959.63
Latitude (°N)	44.018	44.717	44.749
Longitude (°W)	-113.932	-111.197	-111.301
Strike (°N)	152	136	128
Dip (°)	49	50	45
Rake (°)	-90	-90	-90
Amplitude (mm)	2100	7800	7000
Bottom of Fault (km)	13.6	10.2	11.8
Top of Fault (km)	0.0	1.7	0.3
Fault Length (km)	18	18	18

Table S-7. Input parameters to VISCO1D from Nishimura & Thatcher (2003) for the earth model.

Thickness (km)	Density (g/cm^3)	Bulk Modulus (10^{10} Pa)	Shear Modulus (10^{10} Pa)	Viscosity (Pa-s)
5	2.60	7.093	2.569	$1.00x10^{30}$
15	2.67	8.642	3.13	$1.00x10^{30}$
20	3.00	12.067	4.371	$1.00x10^{30}$
100	3.30	18.372	6.654	$4.00x10^{18}$

Table S-8. Results of F distribution tests between post-seismic and preferred model pairs.

Model	χ_η^2	DOF	P (%)
ctb9	1.21	522	100
s1mr	1.53	522	
ctb9	1.21	522	100
s2mr	1.53	519	
ctb9	1.21	522	50
s3mr	1.21	519	
ctb9	1.21	522	91
s4mr	1.36	522	
ctb9	1.21	522	70
s5mr	1.26	522	
ctb9	1.21	522	67
s6mr	1.25	522	

χ_η^2 - Reduced Chi-square; DOF – Degrees of Freedom; P – Probability that misfit variances are from different distributions.
ctb9 is the preferred model.

Plots of Post-seismic Model Results

We show results in the form of residual velocities for how the models fit the corrected GPS velocities. These figures show plots with:

- Pole of rotation (brown dot with 70% confidence ellipse) for poles located within the map region
- Name of a pole (brown letters, e.g. P010 or EWas)
- Residual velocities (gray vectors with 70% confidence ellipses)
- Principal horizontal strain rate axes (pink arrows) and strain rates (pink letters)
- Block model configuration (solid green lines)
- Model name (e.g. nb11) and inversion results listed as C2/NP/DF, which corresponds to reduced chi-square (CD), number of free parameters (NP), and degrees of freedom (DF)
- Name (red letters) of the block (e.g. EWas) or name of the pole that has multiple blocks with the same angular velocity (e.g. P010)
- Reduced chi-square of GPS velocities (red numbers) in each block or for all blocks with the same pole of rotation.

Figures with post-seismic relaxation velocities show:

- Mantle viscosity (MV) that was used to produce the post-seismic relaxation velocities and model names that used them in the inversions
- Post-seismic relaxation velocities at each of the GPS sites (blue vectors)
- Red dots and years show epicenters for the 1983 **M** 6.9 Borah Peak, Idaho (in CTB) and 1959 **M** 7.3 Hebgen Lake, Montana (near YP)
- Acronyms: CSZ – Centennial Shear Zone; CTB – Centennial Tectonic Belt; GB – Great Basin; IB – Idaho Batholith; ISB – Intermountain Seismic Belt; OIG – Oregon-Idaho Graben; OP – Owyhee-Oregon Plateau; RM – Rocky Mountains; SRP – Snake River Plain; YP – Yellowstone Plateau.

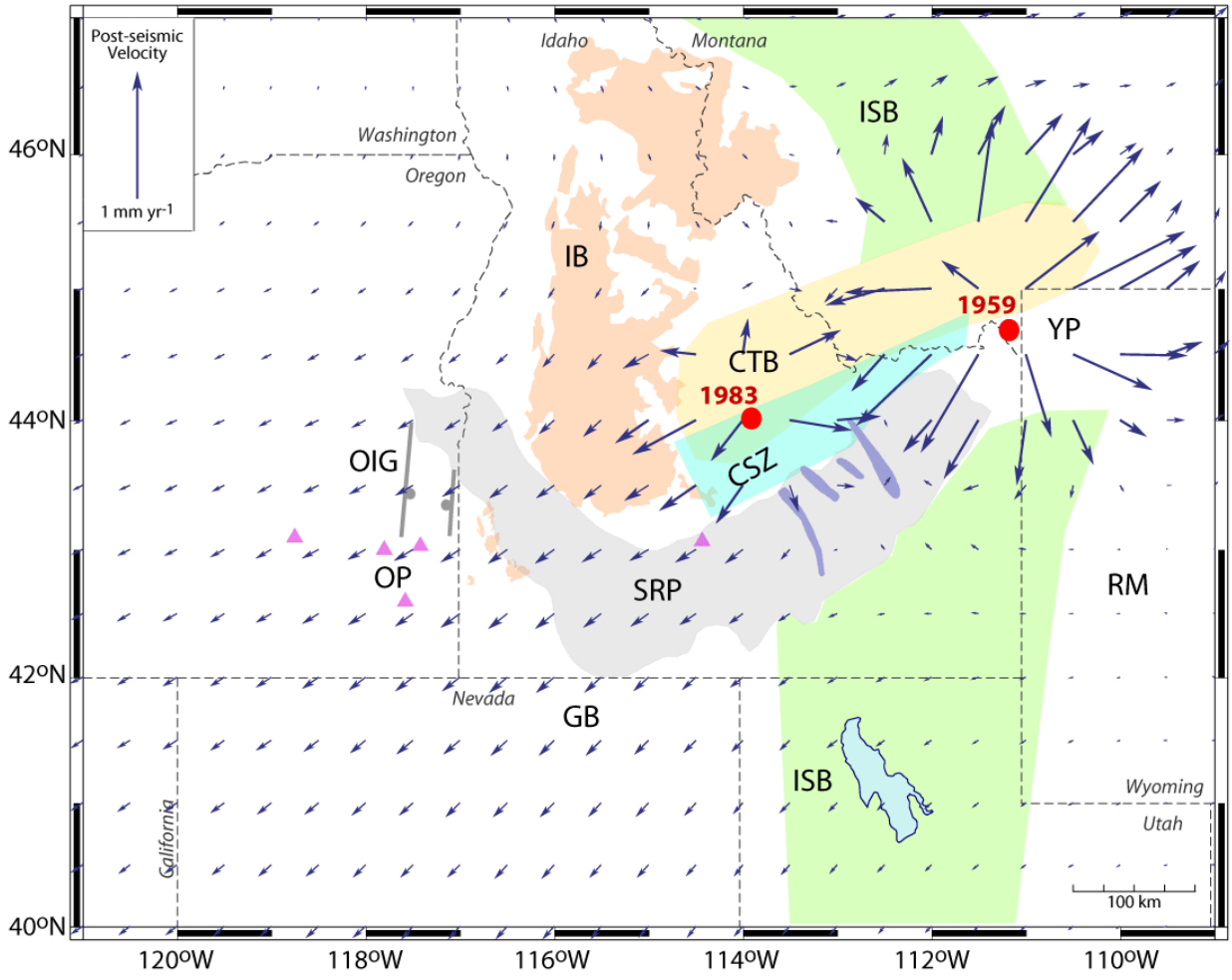

Figure S-11. Plot shows reproduction of synthetic post-seismic velocities from VISCO1D generated using input parameters (e.g. mantle viscosity of $4x10^{17.5}$ Pa-s) from Nishimura & Thatcher (2003). The 1983 Borah Peak, Idaho earthquake is modeled as one planar source and the 1959 Hebgen Lake, Montana earthquake as two planar sources.

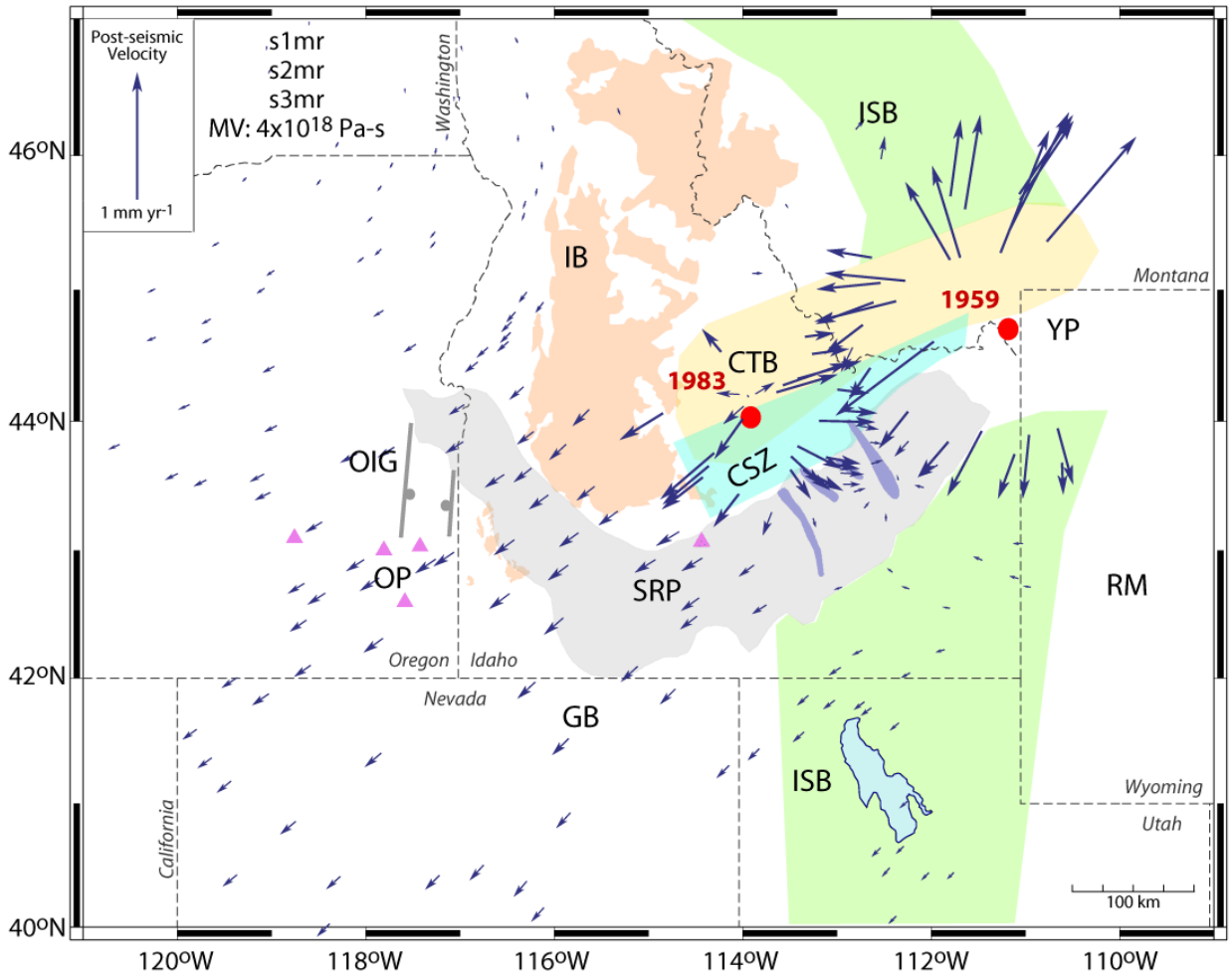

Figure S-12. Plot shows synthetic post-seismic velocities at GPS sites generated using VISCO1D and input parameters (e.g. mantle viscosity of $4x10^{18}$ Pa-s) from Nishimura & Thatcher (2003), which were used to correct the 1994-2010 velocity field for models s1mr, s2mr, and s3mr.

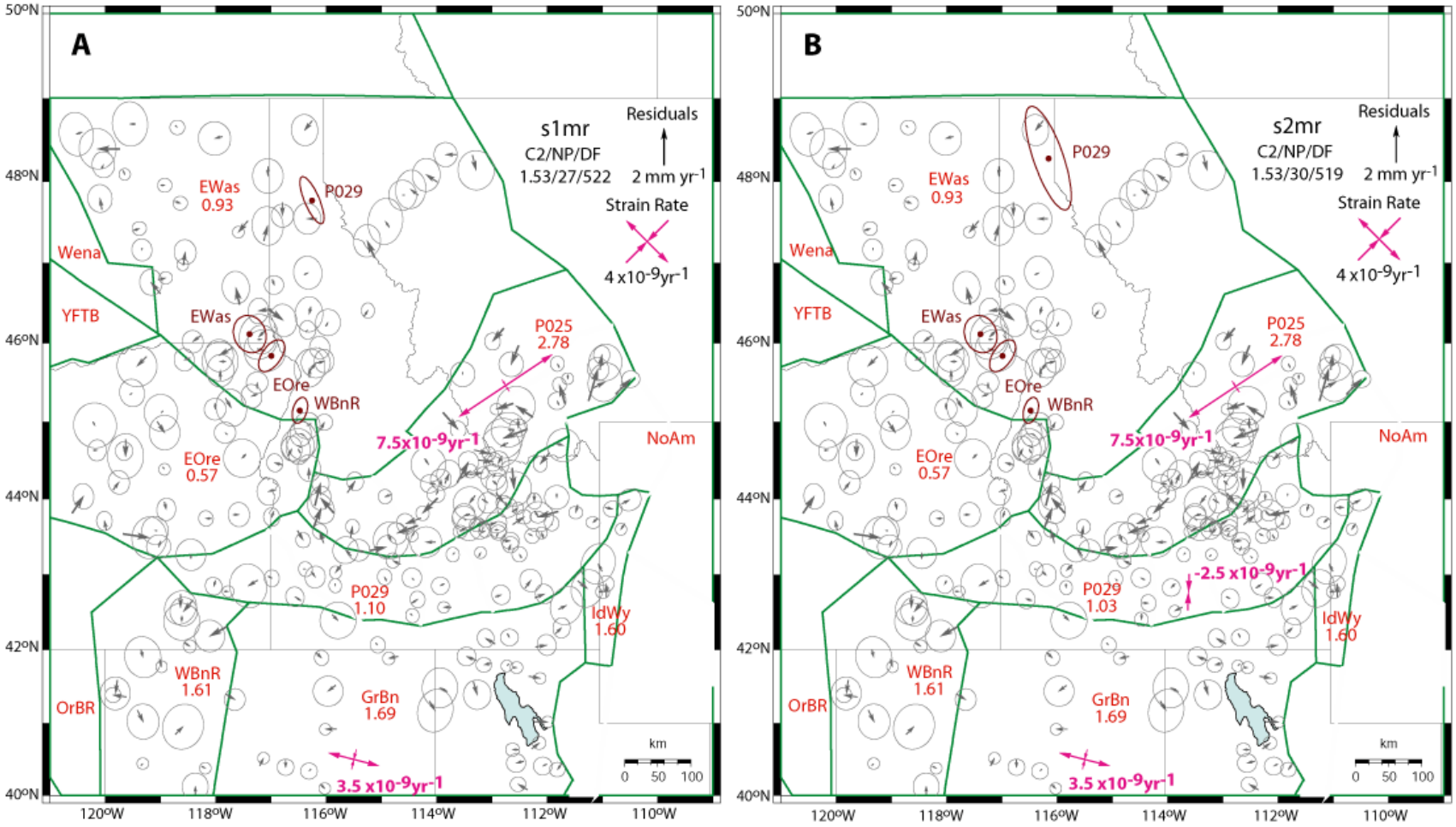

Figure S-13. Models **s1mr** and **s2mr** assume nine poles; pole P025 is for multiple blocks CTBt/SwMT/EMnt/IBat, P029 for blocks ESRP/CSRP/WSRP/Owhy, and all others are individual blocks as labeled (same as ctb9). Results show model fits to the synthetic post-seismic velocities generated for a mantle viscosity of $4x10^{18}$ Pa-s (Nishimura & Thatcher 2003).

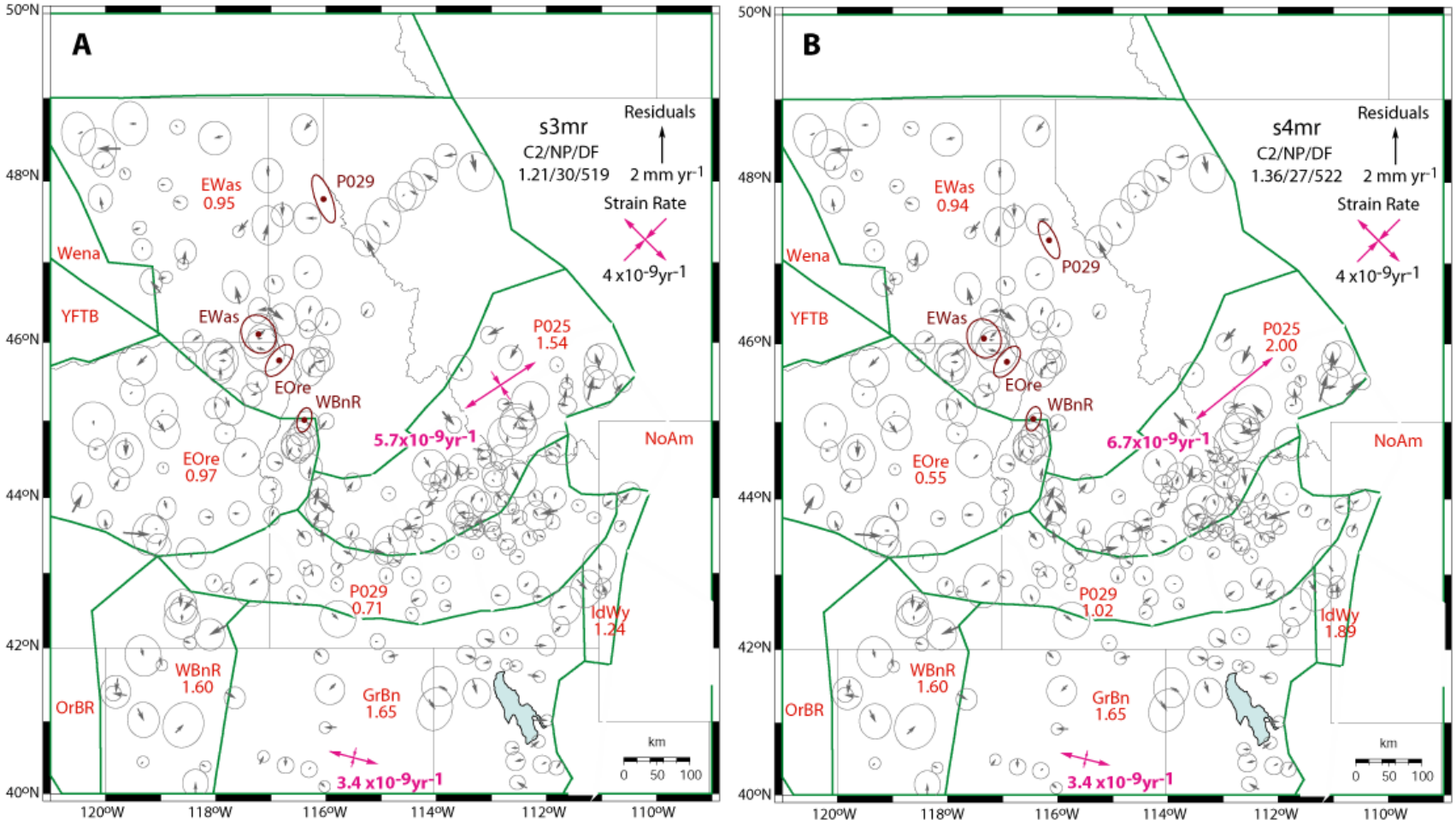

Figure S-14. Models **s3mr** and **s4mr** assume nine poles; pole P025 is for multiple blocks CTBt/SwMT/EMnt/IBat, P029 for blocks ESRP/CSRP/WSRP/Owhy, and all others are individual blocks as labeled (same as ctb9). Model **s3mr** allows earthquake amplitudes to vary for synthetic post-seismic velocities generated for a mantle viscosity of $4x10^{18}$ Pa-s (Nishimura & Thatcher 2003). Model **s4mr** shows results inversions with synthetic post-seismic velocities generated for a mantle viscosity of $4x10^{17.5}$ Pa-s.

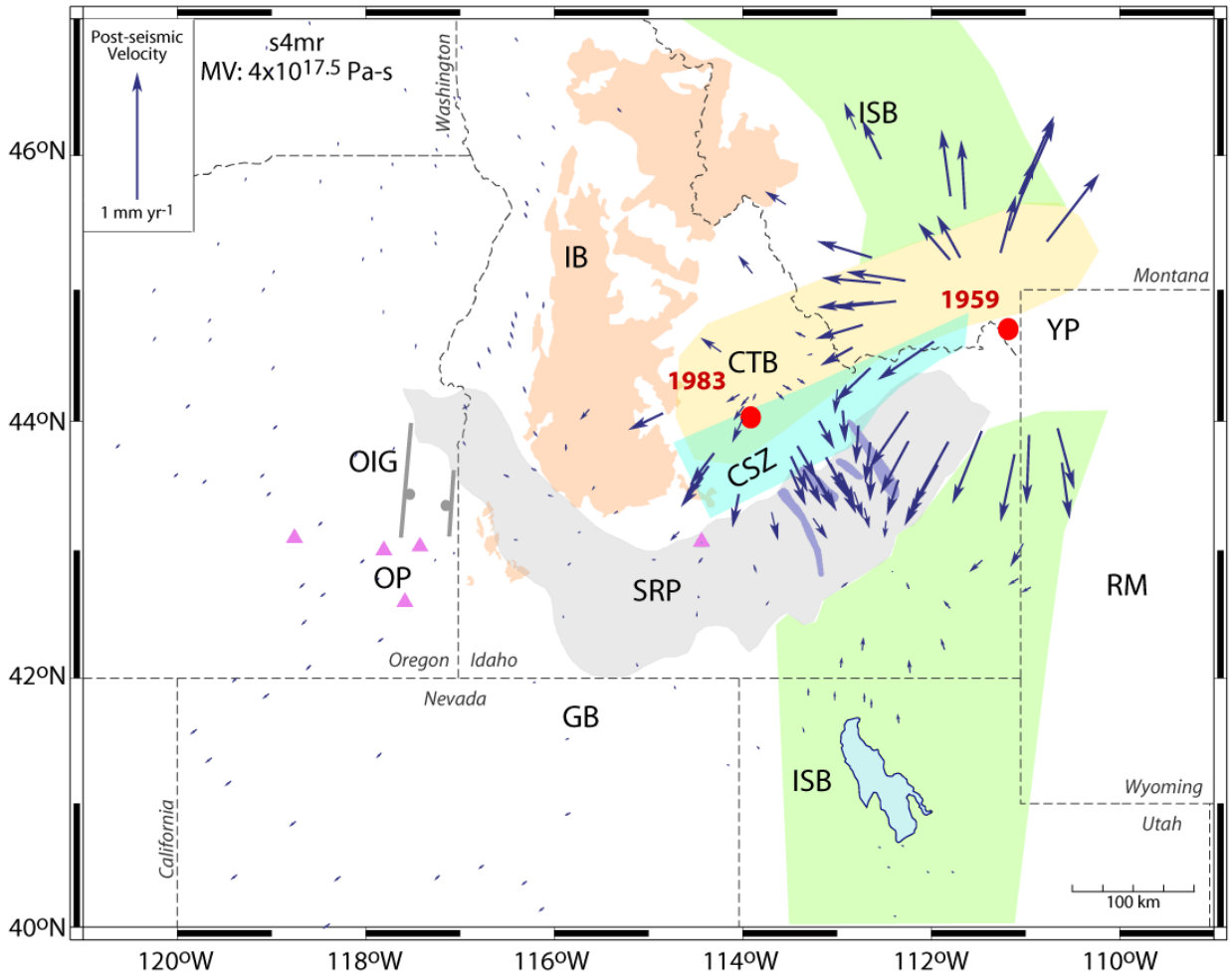

Figure S-15. Plot shows synthetic post-seismic velocities at GPS sites generated using the mantle viscosity of $4x10^{17.5}$ Pa-s, which were used to correct the 1994-2010 velocity field for model s4mr.

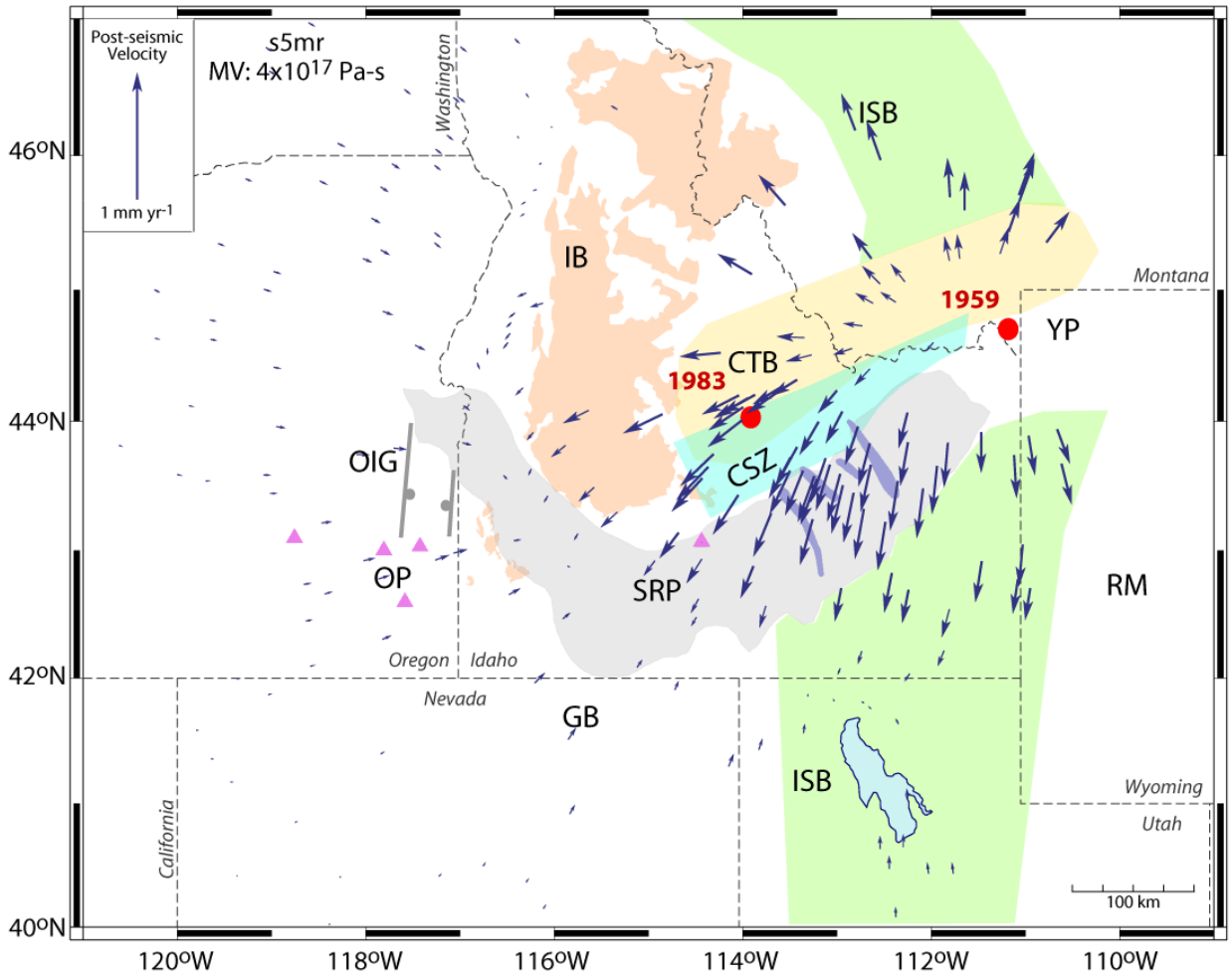

Figure S-16. Plot shows synthetic post-seismic velocities at GPS sites generated using the mantle viscosity of $4x10^{17}$ Pa-s, which were used to correct the 1994-2010 velocity field for model s5mr.

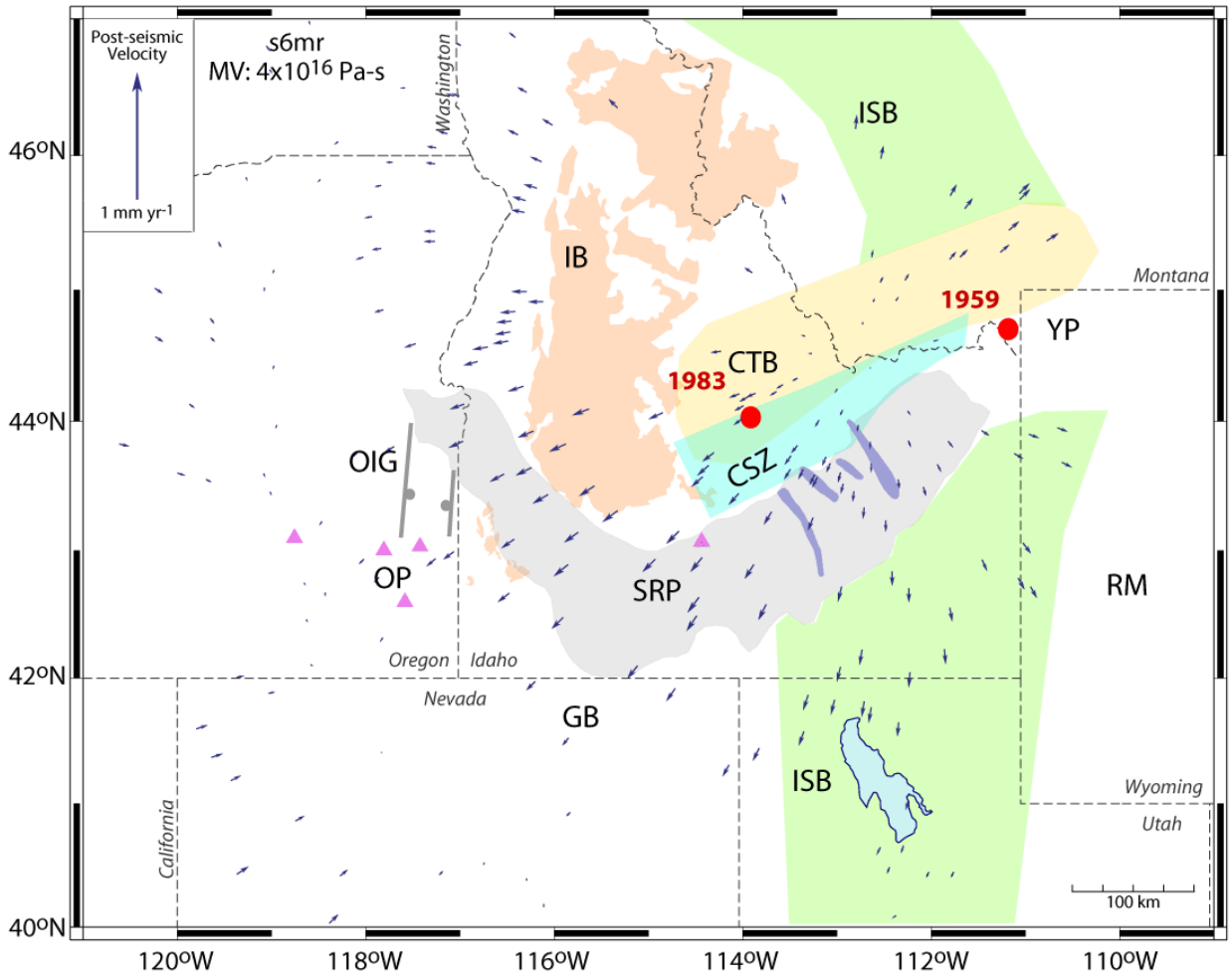

Figure S-17. Plot shows synthetic post-seismic velocities at GPS sites generated using the mantle viscosity of $4x10^{16}$ Pa-s, which were used to correct the 1994-2010 velocity field for model s6mr.

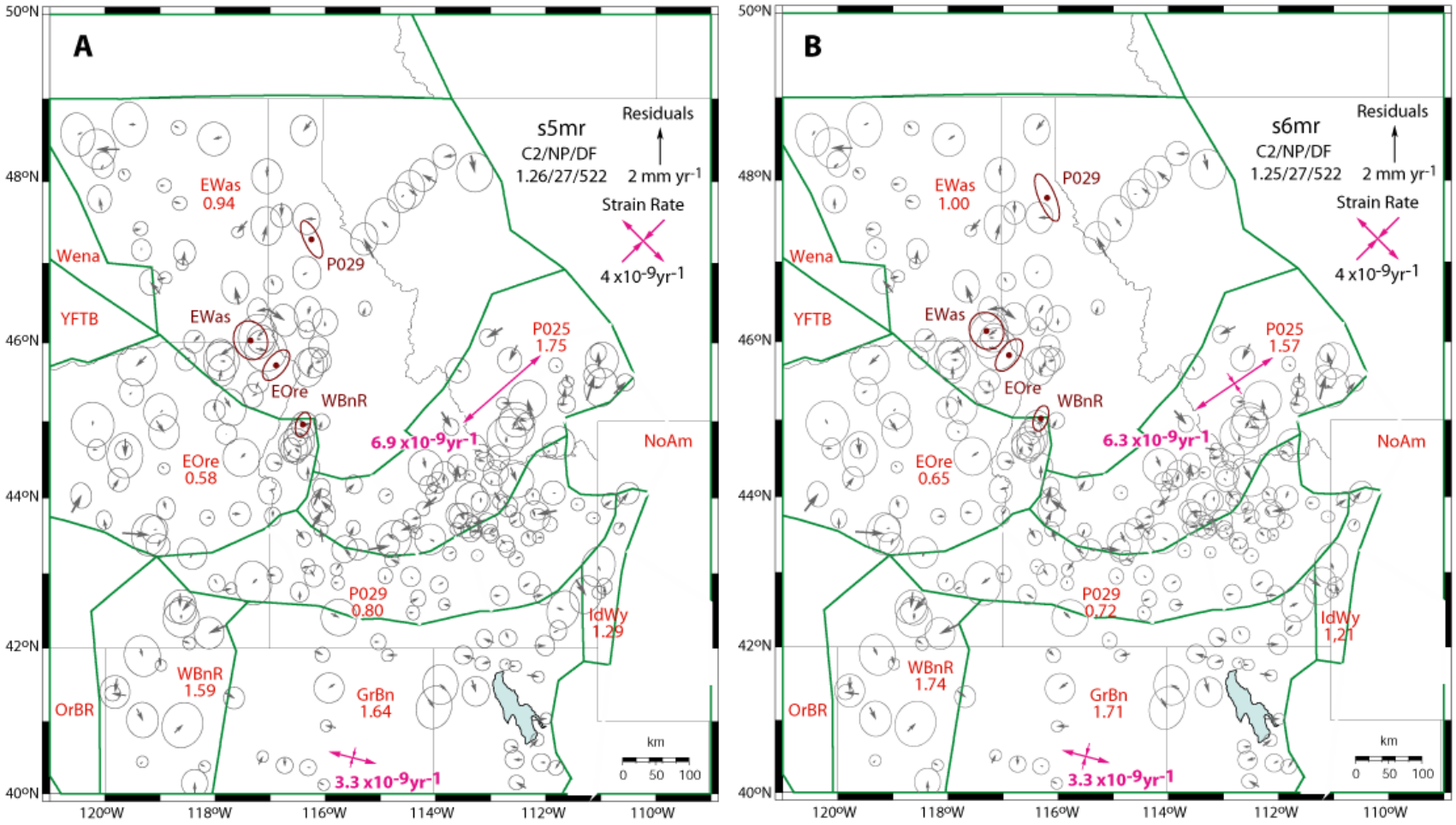

Figure S-18. Models **s5mr** and **s6mr** assume nine poles; pole P025 is for multiple blocks CTBt/SwMT/EMnt/IBat, P029 for blocks ESRP/CSRP/WSRP/Owhy, and all others are individual blocks as labeled (same as ctb9). Model **s5mr** shows results of inversions with synthetic post-seismic velocities generated for a mantle viscosity of $4x10^{17}$ Pa-s and model **s6mr** for a mantle viscosity of $4x10^{16}$ Pa-s.

1994-2010 Horizontal GPS Velocity Field

405 horizontal GPS velocities from the 1994-2010 velocity field (informally referred to as 110429a.vel), which were used in the analyses, are listed in Table S-9. The GPS velocities are shown in Fig. 2 of the manuscript (also see Sections 3.1 and 3.2).

Table S-9. Horizontal GPS velocities in the Stable North American Reference Frame (SNARF).

Longitude ºE	Latitude ºN	East Velocity (mm/yr)	North Velocity (mm/yr)	East Sigma (mm/yr)	North Sigma (mm/yr)	East-North Correlation	GPS Site
245.650	43.647	-3.19	-0.91	0.34	0.37	-0.070	008A
238.742	41.671	-4.94	3.94	0.51	0.58	-0.017	0209
239.634	40.799	-5.70	5.55	0.51	0.59	0.011	0220
244.168	41.511	-4.05	-0.45	0.52	0.52	0.005	036C
246.778	43.579	-2.71	-1.04	0.34	0.34	0.007	0Z36
249.386	44.612	0.27	-0.73	0.28	0.27	-0.011	10RD
243.534	42.656	-3.13	0.41	0.32	0.34	-0.064	16EM
243.897	44.896	-0.15	0.12	0.28	0.28	0.003	187R
239.335	47.768	1.93	1.56	0.59	0.65	-0.014	1882
238.095	46.542	2.49	4.13	0.39	0.47	0.026	217U
246.323	43.292	-2.69	-0.92	0.23	0.25	-0.018	32FM
240.017	43.590	-1.95	2.26	0.27	0.33	-0.016	47EC
246.807	43.558	-2.50	-0.99	0.22	0.23	0.027	5223
240.581	41.173	-4.31	1.90	0.55	0.61	-0.017	74LR
245.299	41.905	-3.88	-0.51	0.21	0.22	0.003	88JD
247.019	44.236	-1.52	-0.75	0.37	0.39	0.003	A038
250.429	43.511	0.01	-0.33	0.46	0.46	0.023	A047
238.825	43.313	-1.22	3.82	0.50	0.57	-0.039	A074
239.575	48.594	0.60	0.67	0.59	0.75	-0.082	A515
239.257	45.475	0.09	2.40	0.55	0.56	-0.013	A545
241.549	43.216	-2.61	1.15	0.51	0.54	-0.013	A699
247.530	43.223	-2.79	-1.36	0.26	0.26	-0.001	ABDI
247.050	43.595	-2.50	-1.27	0.29	0.29	0.000	AECU
248.936	42.773	-0.99	-1.13	0.24	0.23	0.001	AHID
244.842	37.358	-3.36	-0.11	0.15	0.14	0.002	ALAM
281.929	45.956	-0.09	-0.77	0.15	0.16	0.016	ALGO
240.001	42.954	-2.93	2.74	0.24	0.26	-0.040	ALKA
238.253	42.209	-3.24	4.50	0.32	0.39	-0.092	ALTA
242.877	46.148	-0.30	-0.33	0.67	0.78	0.035	ANAT
245.976	44.198	-2.06	-0.65	0.32	0.32	0.037	ANDF
245.068	36.319	-3.18	0.11	0.16	0.15	0.001	APEX
247.377	43.667	-1.97	-1.03	0.26	0.25	-0.001	ARNG
241.529	45.813	-0.34	0.23	0.35	0.39	-0.040	ATHE
241.271	40.848	-4.53	2.37	0.71	0.78	0.085	B073
240.273	46.578	0.39	1.13	0.64	0.67	-0.006	B317

Table S-9. Continued.

Longitude ºE	Latitude ºN	East Velocity (mm/yr)	North Velocity (mm/yr)	East Sigma (mm/yr)	North Sigma (mm/yr)	East-North Correlation	GPS Site
242.795	40.413	-3.91	0.57	0.18	0.17	0.000	BAMO
248.951	45.707	0.21	-0.43	0.57	0.63	0.019	BASE
248.157	42.215	-2.38	-0.74	0.30	0.35	0.027	BATI
248.474	44.185	-2.01	-2.15	0.23	0.22	-0.004	BBID
246.594	44.316	-1.43	-0.67	0.19	0.18	0.000	BCYI
248.954	44.149	-2.08	-2.00	0.59	0.52	0.026	BECH
247.243	43.960	-1.62	-0.84	0.35	0.35	-0.005	BIRC
242.192	42.307	-4.13	0.72	0.52	0.55	-0.010	BLMT
250.442	42.767	-0.08	0.18	0.47	0.45	-0.004	BLWY
243.742	48.731	0.50	-0.71	0.46	0.54	-0.033	BNRS
243.598	46.857	0.43	-0.12	0.49	0.57	-0.048	BOVL
248.954	45.663	-0.07	0.17	0.28	0.31	0.013	BOZE
240.317	48.132	0.82	0.41	0.17	0.16	0.003	BREW
295.304	32.370	0.62	0.29	0.30	0.30	0.045	BRMU
295.304	32.370	1.06	0.03	0.33	0.34	0.085	BRMU
239.400	43.814	-1.10	3.03	0.36	0.44	-0.059	BROT
242.156	42.780	-2.63	0.76	0.16	0.14	0.000	BURN
247.662	43.540	-2.31	-1.67	0.26	0.26	0.025	BUSH
247.482	45.968	-0.43	-1.36	0.42	0.43	-0.003	BUTT
246.821	43.998	-1.86	-0.82	0.34	0.36	0.014	C054
242.431	46.486	-0.09	0.95	0.47	0.56	-0.045	C334
247.175	44.553	-1.33	-0.72	0.39	0.44	0.041	CABI
243.307	44.555	-0.80	0.28	0.36	0.43	-0.034	CAMB
249.323	39.191	-0.84	-0.08	0.15	0.13	0.003	CAST
240.451	45.344	-0.26	1.66	0.43	0.48	-0.064	CBL1
241.411	46.973	0.39	1.00	0.38	0.43	-0.045	CC25
265.911	58.759	-0.43	-0.91	0.22	0.22	-0.011	CHUR
246.655	43.619	-2.51	-0.54	0.44	0.44	0.002	CIND
247.367	43.830	-2.15	-1.25	0.20	0.20	0.004	CIRC
243.601	44.824	-1.01	-0.15	0.37	0.45	-0.025	CNID
247.080	43.508	-2.59	-1.12	0.26	0.26	0.000	COBB
243.204	47.743	0.57	-0.77	0.38	0.40	-0.009	COEU
242.180	45.297	-0.15	0.06	0.53	0.64	-0.082	COVE
246.527	43.723	-2.35	-0.40	0.41	0.42	0.000	CRAW
239.740	46.979	1.70	1.56	0.72	0.77	-0.021	CRBT
248.644	44.656	-1.71	-2.93	0.60	0.59	-0.019	D092
241.068	43.960	-1.39	0.77	0.33	0.39	0.053	D706
238.825	45.618	0.74	2.74	0.27	0.32	-0.032	DALL
246.593	43.803	-2.62	-0.64	0.39	0.42	0.020	DARI
247.385	45.232	-1.11	-0.68	0.21	0.19	0.010	DILL
246.440	44.266	-1.65	-0.39	0.22	0.24	-0.010	DONK
246.370	44.214	-1.64	0.29	0.35	0.37	0.001	DONP
247.787	42.036	-2.15	-0.87	0.33	0.36	-0.058	DRUF

Table S-9. Continued.

Longitude ºE	Latitude ºN	East Velocity (mm/yr)	North Velocity (mm/yr)	East Sigma (mm/yr)	North Sigma (mm/yr)	East-North Correlation	GPS Site
264.134	50.259	-1.22	-1.46	0.24	0.23	-0.003	DUBO
239.820	45.243	0.33	1.14	0.52	0.63	-0.024	E040
243.588	43.075	-2.54	0.13	0.24	0.26	-0.055	E072
248.042	44.598	-1.66	-1.76	0.24	0.27	-0.013	E138
239.408	47.559	2.15	1.82	0.65	0.80	-0.060	E518
245.736	37.916	-3.36	-0.50	0.16	0.15	0.002	ECHO
245.061	39.345	-4.23	-0.38	0.16	0.15	0.001	EGAN
242.083	45.533	-0.15	0.72	0.47	0.56	0.023	ELGN
242.298	45.937	-0.73	-0.28	0.49	0.56	-0.012	ELKF
244.183	40.915	-4.28	-0.08	0.14	0.13	0.001	ELKO
247.073	44.074	-1.42	-1.03	0.26	0.25	0.000	EMIG
246.361	48.326	0.16	-0.98	0.40	0.42	0.002	ESEX
248.988	43.048	-1.39	-0.77	0.59	0.70	0.126	ETNA
248.217	45.692	-0.16	-0.56	0.24	0.26	0.005	F145
246.191	41.430	-3.54	-0.36	0.61	0.69	0.002	F381
243.551	44.669	-1.12	-0.09	0.57	0.58	-0.007	F408
243.881	45.942	-0.05	-0.28	0.35	0.39	-0.029	FAAS
238.867	46.629	1.33	1.74	0.50	0.54	0.019	FALL
241.358	42.739	-2.74	1.15	0.55	0.58	0.111	FLAK
244.685	46.339	0.24	-0.16	0.23	0.26	-0.011	FLAT
258.022	54.726	-0.86	-1.75	0.18	0.17	-0.023	FLIN
246.195	39.369	-3.53	-0.42	0.17	0.15	0.002	FOOT
239.780	45.000	-0.63	1.73	0.74	0.78	-0.023	FOSS
247.501	36.988	-1.72	-0.25	0.15	0.14	0.003	FRED
248.750	45.269	0.02	0.57	0.37	0.40	-0.085	G103
247.288	44.726	-1.09	-0.38	0.68	0.70	0.012	G318
238.731	48.674	2.09	1.94	0.41	0.49	-0.045	G370
243.627	46.142	0.10	-0.10	0.28	0.32	-0.026	G404
242.175	41.398	-3.80	0.91	0.36	0.38	0.004	G425
242.084	38.970	-4.31	1.01	0.15	0.14	-0.001	GABB
240.645	40.417	-5.34	2.58	0.14	0.13	-0.001	GARL
241.923	43.744	-1.94	0.72	0.25	0.27	-0.034	GENT
246.749	44.504	-0.92	-0.67	0.32	0.32	0.036	GILM
239.185	45.839	0.83	2.13	0.15	0.14	0.004	GOBS
283.173	39.022	0.24	-0.23	0.15	0.15	0.058	GODE
248.556	42.919	-1.98	-1.63	0.56	0.65	0.106	GRA5
246.944	43.665	-2.28	-1.09	0.36	0.36	-0.005	GRAF
248.212	42.541	-2.25	-0.91	0.56	0.66	0.135	GRCE
246.759	43.244	-2.59	-0.95	0.16	0.14	0.000	GTRG
238.672	45.783	1.78	2.58	0.19	0.18	0.003	GWEN
243.795	43.913	-2.52	0.29	0.30	0.34	-0.023	H015
241.427	42.094	-3.17	1.67	0.22	0.23	-0.041	H118
248.321	45.232	-0.37	0.11	0.24	0.26	-0.060	H146

Table S-9. Continued.

Longitude ºE	Latitude ºN	East Velocity (mm/yr)	North Velocity (mm/yr)	East Sigma (mm/yr)	North Sigma (mm/yr)	East-North Correlation	GPS Site
243.813	41.962	-3.46	-0.42	0.25	0.26	-0.013	H318
245.871	41.296	-2.98	-0.97	0.62	0.74	0.113	H348
245.550	42.624	-2.59	-0.46	0.26	0.29	-0.040	H422
249.111	44.640	-5.66	-2.60	0.72	0.74	-0.013	HARL
248.627	40.514	-1.16	-0.36	0.15	0.14	0.003	HEBE
244.786	43.318	-2.09	-0.81	0.35	0.40	0.078	HIL5
245.586	43.563	-2.28	-0.79	0.15	0.14	0.001	HLID
240.741	45.827	-0.50	0.84	0.69	0.71	-0.007	HMIS
246.900	43.713	-2.64	-0.83	0.26	0.25	0.002	HPIG
251.330	44.013	-0.53	0.14	0.61	0.69	0.123	HSWY
248.435	41.607	-0.88	-0.41	0.22	0.20	0.003	HWUT
247.932	43.481	-2.64	-1.42	0.19	0.19	-0.028	I107
247.764	44.068	-2.03	-1.73	0.25	0.28	-0.044	I132
247.599	42.826	-2.61	-1.15	0.38	0.39	-0.042	I585
247.778	42.696	-2.52	-1.43	0.31	0.34	-0.060	I762
247.059	44.330	-1.47	-0.76	0.44	0.44	0.005	ICIG
243.770	43.634	-2.67	0.07	0.47	0.52	-0.227	IDT1
243.004	46.428	-0.60	-0.16	0.35	0.44	0.055	IDT2
239.479	47.012	0.93	0.71	0.58	0.63	0.003	IOOF
240.143	44.119	-1.09	2.17	0.37	0.41	-0.057	J090
243.687	44.254	-1.18	0.33	0.40	0.46	-0.049	J146
249.050	43.890	-1.89	-1.68	0.32	0.28	-0.002	JNWY
240.372	44.623	-1.05	1.60	0.30	0.32	-0.010	JONY
242.947	42.980	-2.47	0.34	0.26	0.29	-0.013	JORD
242.748	45.349	-0.53	-0.05	0.36	0.41	-0.045	JOSE
240.067	42.930	-2.41	2.52	0.31	0.34	-0.063	JUMT
242.941	48.179	0.68	-0.58	0.53	0.60	-0.005	JUSW
248.486	44.598	-2.11	-4.31	0.73	0.75	-0.013	K092
245.664	47.836	0.20	-0.45	0.52	0.67	0.052	K443
243.995	46.213	0.10	-0.07	0.43	0.46	0.001	KAMI
309.055	66.987	-2.66	0.34	0.29	0.30	0.006	KELY
309.055	66.987	1.12	0.37	0.67	0.67	-0.005	KELY
244.451	43.252	-2.97	0.03	0.44	0.47	0.031	KT05
248.695	44.317	-2.22	-2.72	0.59	0.59	-0.011	L011
246.468	45.629	-0.66	-0.45	0.42	0.43	-0.003	L070
239.937	47.656	0.46	1.25	0.42	0.48	-0.028	L387
249.805	42.271	-0.88	0.04	0.28	0.29	0.006	LABA
246.673	44.637	-0.78	-0.76	0.23	0.24	-0.049	LEAD
249.365	44.267	-1.93	-0.10	0.36	0.39	-0.114	LEWF
239.462	47.000	1.13	1.25	0.17	0.16	0.005	LIND
244.386	44.083	-2.06	-0.16	0.29	0.32	-0.043	LOMN
240.646	41.997	-3.46	2.07	0.63	0.71	-0.070	LOPE
242.868	47.274	0.62	0.77	0.54	0.67	-0.043	LTAH

Table S-9. Continued.

Longitude ºE	Latitude ºN	East Velocity (mm/yr)	North Velocity (mm/yr)	East Sigma (mm/yr)	North Sigma (mm/yr)	East-North Correlation	GPS Site
244.809	36.159	-2.77	-0.29	0.35	0.34	0.001	LVWD
251.786	43.586	0.29	0.51	0.68	0.75	0.091	M327
245.088	42.923	-2.78	-0.26	0.25	0.28	-0.011	M413
240.364	44.772	-0.83	0.71	0.62	0.78	0.017	M415
247.796	47.834	0.24	-0.28	0.59	0.67	0.041	M729
246.644	48.317	0.95	-1.81	0.63	0.68	-0.010	MARI
249.670	42.714	-0.86	-0.58	0.34	0.34	-0.009	MASN
249.311	44.973	0.28	-0.16	0.14	0.13	-0.001	MAWY
238.778	42.418	-2.96	4.07	0.20	0.19	0.000	MDMT
255.985	30.681	-0.55	-0.41	0.14	0.13	0.033	MDO1
240.993	46.621	-0.31	1.01	0.39	0.45	-0.033	MESA
241.585	42.660	-3.33	1.07	0.47	0.49	-0.003	MICK
243.904	40.148	-3.63	-0.12	0.20	0.19	-0.002	MINE
243.284	39.148	-3.78	0.13	0.15	0.14	0.000	MONI
248.366	40.016	-1.15	-0.16	0.24	0.23	0.012	MPUT
238.458	46.000	1.46	4.13	0.47	0.50	-0.016	MTAD
249.144	44.819	-0.64	2.49	0.67	0.67	0.000	MTHM
244.872	47.067	-0.11	0.42	0.47	0.56	0.027	MTID
247.302	43.326	-2.57	-1.19	0.28	0.28	-0.009	N056
248.521	44.830	-0.73	-0.74	0.25	0.27	0.011	N144
243.045	43.835	-1.66	-0.22	0.28	0.32	-0.034	N417
239.332	40.418	-7.63	5.50	0.45	0.46	-0.069	N843
247.770	41.016	-2.13	-0.77	0.15	0.14	0.002	NAIU
242.491	39.686	-4.21	0.30	0.15	0.13	-0.001	NEWS
247.054	42.078	-3.43	-0.54	0.29	0.32	-0.040	NGRI
268.425	41.772	-0.08	0.13	0.16	0.16	0.010	NLIB
243.720	44.974	-0.89	-0.43	0.45	0.46	0.001	NMDS
248.370	45.597	-0.09	-1.10	0.16	0.14	0.005	NOMT
249.322	44.715	-1.51	-3.23	0.32	0.30	0.003	NRWY
251.522	43.066	0.04	-0.76	0.48	0.49	0.015	NWS1
245.166	44.054	-2.29	-0.67	0.24	0.25	-0.023	OBSN
239.276	46.951	1.36	1.44	0.19	0.18	0.004	OBSV
249.168	44.452	-1.87	-3.47	0.31	0.28	0.001	OFWY
241.039	44.410	-1.08	1.09	0.18	0.18	-0.006	OGIL
243.719	46.455	0.00	-0.66	0.48	0.61	0.027	OROF
242.813	39.521	-4.02	0.25	0.29	0.28	0.004	P002
244.721	39.910	-3.91	-0.45	0.29	0.28	0.002	P005
247.777	38.480	-2.36	-0.21	0.27	0.26	0.003	P009
247.639	40.078	-3.41	-0.36	0.27	0.25	0.002	P016
244.688	43.300	-2.79	-0.21	0.38	0.37	0.006	P019
241.434	47.002	0.16	0.24	0.20	0.19	0.002	P020
241.270	48.675	1.03	0.22	0.26	0.25	0.005	P021
241.986	45.232	-0.45	0.32	0.38	0.37	0.006	P022

Table S-9. Continued.

Longitude ºE	Latitude ºN	East Velocity (mm/yr)	North Velocity (mm/yr)	East Sigma (mm/yr)	North Sigma (mm/yr)	East-North Correlation	GPS Site
249.487	41.750	-1.12	-0.14	0.24	0.23	0.003	P030
247.377	41.757	-2.64	-0.83	0.22	0.20	0.002	P057
238.909	43.112	-2.27	3.70	0.42	0.41	0.005	P062
239.054	44.923	0.07	2.62	0.27	0.29	-0.012	P063
239.067	46.844	1.67	1.72	0.31	0.30	0.004	P065
242.015	39.306	-4.57	1.00	0.31	0.30	0.002	P068
242.599	39.347	-4.22	0.25	0.29	0.28	0.001	P071
243.259	39.521	-4.07	0.14	0.23	0.22	0.002	P072
243.576	39.501	-3.85	0.00	0.29	0.27	0.004	P073
243.950	39.546	-3.81	-0.25	0.29	0.27	0.003	P074
244.111	39.374	-3.98	-0.18	0.31	0.29	0.003	P075
244.487	39.536	-3.95	-0.35	0.29	0.28	0.004	P076
245.723	39.119	-3.88	-0.29	0.29	0.28	0.004	P080
243.264	40.495	-3.96	-0.29	0.29	0.28	0.004	P085
247.718	40.649	-2.41	-0.43	0.23	0.22	0.002	P086
243.721	40.363	-4.01	-0.01	0.29	0.28	0.003	P087
248.277	40.772	-1.03	-0.52	0.28	0.26	0.003	P088
241.841	39.212	-4.72	1.87	0.30	0.29	0.002	P099
246.706	41.857	-3.58	-0.51	0.33	0.32	0.005	P100
248.764	41.692	-1.02	-0.36	0.24	0.23	0.003	P101
244.444	39.925	-4.00	-0.25	0.29	0.27	0.004	P102
247.283	39.186	-3.09	-0.14	0.27	0.25	0.004	P104
247.738	39.459	-3.13	-0.52	0.27	0.25	0.003	P106
248.055	39.589	-2.44	-0.23	0.26	0.24	0.005	P108
248.349	39.597	-1.69	-0.17	0.42	0.41	0.006	P109
248.429	39.715	-2.11	-0.47	0.45	0.45	0.006	P110
246.988	41.817	-3.33	-0.82	0.27	0.25	0.003	P111
248.550	39.817	-1.20	-0.38	0.27	0.25	0.003	P112
247.472	40.634	-3.17	-0.67	0.24	0.23	0.004	P114
247.572	40.474	-3.30	-0.76	0.33	0.32	0.004	P115
247.986	40.434	-2.94	-0.85	0.32	0.31	0.004	P116
248.249	40.435	-2.93	-1.12	0.27	0.25	0.009	P117
248.650	40.635	-0.94	-0.35	0.27	0.25	0.003	P118
248.742	40.732	-1.09	-0.22	0.23	0.21	0.001	P119
247.302	41.803	-3.00	-0.90	0.20	0.19	0.002	P121
247.668	41.635	-2.19	-0.98	0.20	0.19	0.001	P122
240.931	39.486	-6.26	3.03	0.31	0.30	0.003	P128
240.376	41.358	-5.10	2.80	0.27	0.26	0.002	P145
245.137	43.533	-2.58	-1.19	0.61	0.64	0.006	P350
246.021	44.109	-1.92	-0.79	0.31	0.29	0.003	P354
248.549	44.318	-2.14	-2.89	0.23	0.22	0.002	P360
242.748	45.428	-0.21	0.28	0.37	0.37	0.006	P372
238.220	42.260	-3.39	4.58	0.37	0.36	0.003	P380

Table S-9. Continued.

Longitude ºE	Latitude ºN	East Velocity (mm/yr)	North Velocity (mm/yr)	East Sigma (mm/yr)	North Sigma (mm/yr)	East-North Correlation	GPS Site
240.048	43.002	-1.63	2.87	0.42	0.41	0.003	P381
238.230	43.177	-0.74	4.70	0.66	0.69	0.004	P382
238.426	44.297	2.01	3.35	0.40	0.40	0.005	P387
239.622	42.469	-3.81	3.18	0.39	0.38	0.002	P388
240.999	43.447	-2.06	0.91	0.42	0.41	0.004	P392
242.200	44.835	-0.85	0.59	0.37	0.36	0.004	P394
243.020	46.798	0.35	-0.33	0.33	0.32	0.003	P422
238.317	46.623	2.03	2.46	0.20	0.19	0.003	P432
238.924	47.740	2.15	1.81	0.49	0.49	0.007	P434
238.714	48.510	2.39	2.43	0.55	0.57	0.009	P443
239.328	45.590	0.60	2.31	0.38	0.37	0.003	P445
239.995	45.911	0.60	1.39	0.39	0.39	0.005	P448
240.369	46.260	0.64	1.21	0.27	0.26	0.003	P449
240.456	45.953	0.46	1.20	0.24	0.23	0.003	P450
240.959	46.793	0.59	0.58	0.23	0.21	0.002	P451
240.513	47.404	0.79	0.62	0.25	0.24	0.008	P452
241.255	47.759	0.84	0.25	0.25	0.24	0.004	P453
241.007	47.954	0.86	0.45	0.25	0.24	0.003	P454
248.775	44.863	0.76	0.45	0.50	0.50	0.010	P456
248.727	45.041	-0.67	1.78	0.33	0.32	0.003	P457
248.971	45.140	0.17	0.29	0.32	0.30	0.004	P460
249.241	45.354	0.31	-0.15	0.31	0.29	0.003	P461
247.281	42.212	-2.78	-1.02	0.31	0.29	0.004	P675
248.662	44.654	-1.37	-3.58	0.44	0.43	0.001	P676
246.132	42.879	-2.94	-0.91	0.31	0.30	0.003	P677
247.195	43.449	-2.29	-1.38	0.31	0.29	0.003	P678
246.694	44.040	-2.04	-1.01	0.56	0.57	0.010	P679
248.901	44.598	-0.98	-3.19	0.30	0.29	0.003	P680
247.364	44.400	-1.01	-1.30	0.61	0.60	0.001	P681
248.550	43.919	-2.19	-1.81	0.24	0.22	0.002	P684
248.170	44.068	-2.25	-1.95	0.42	0.41	0.004	P685
248.845	44.252	-1.89	-2.71	0.36	0.35	0.006	P686
247.476	45.043	-0.25	-0.83	0.31	0.30	0.003	P706
248.163	44.719	-1.49	-1.90	0.57	0.57	0.004	P707
248.928	44.957	-0.17	1.45	0.27	0.27	-0.027	P712
250.310	43.501	-0.55	-0.32	0.31	0.30	0.003	P715
250.624	44.753	-0.17	-0.50	0.32	0.30	0.004	P718
248.211	45.218	-0.01	-0.69	0.31	0.30	0.003	P719
249.694	44.943	-0.03	0.14	0.34	0.33	-0.004	P720
249.998	45.003	-0.10	-0.13	0.35	0.35	0.004	P721
250.429	45.457	-0.07	-0.53	0.31	0.30	0.005	P722
248.585	40.808	-1.02	-0.27	0.26	0.25	0.005	P783
243.951	43.426	-2.60	0.66	0.25	0.26	-0.021	P84R

Table S-9. Continued.

Longitude ºE	Latitude ºN	East Velocity (mm/yr)	North Velocity (mm/yr)	East Sigma (mm/yr)	North Sigma (mm/yr)	East-North Correlation	GPS Site
238.325	46.607	2.42	3.47	0.43	0.47	0.015	PACK
249.807	44.648	-1.06	0.47	0.45	0.45	-0.001	PELI
238.717	44.061	-0.47	3.10	0.45	0.51	-0.070	PIBU
251.881	34.302	-1.28	0.03	0.32	0.16	0.001	PIE1
251.881	34.302	-0.76	-0.97	0.28	0.25	0.014	PIE1
251.881	34.302	-1.14	0.03	0.21	0.16	0.010	PIE1
243.732	43.044	-2.57	-0.25	0.35	0.38	0.048	PITT
242.179	45.769	-0.39	0.15	0.62	0.68	-0.007	PLMR
243.056	44.119	-1.58	-0.03	0.40	0.47	-0.015	PNAZ
245.707	50.871	0.57	-1.39	0.38	0.37	0.001	PRDS
245.707	50.871	-0.02	-2.36	0.24	0.23	-0.002	PRDS
247.642	44.906	-1.39	-0.68	0.67	0.69	0.001	PRIC
239.135	44.301	-0.73	4.08	0.59	0.66	-0.066	PRIN
242.315	43.794	-1.27	0.50	0.37	0.42	-0.020	PSTP
249.191	39.599	-0.76	-0.73	0.16	0.15	0.004	PUC1
240.322	43.539	-0.46	1.47	0.60	0.72	0.022	Q374
250.849	44.838	0.36	0.46	0.63	0.68	0.107	Q84X
249.610	44.890	0.74	0.71	0.39	0.39	0.003	R011
246.073	44.179	-1.85	-0.44	0.36	0.36	-0.018	R015
242.751	45.929	0.38	-0.13	0.72	0.73	-0.013	R409
242.543	44.578	-1.20	0.14	0.64	0.66	-0.001	R489
244.335	38.280	-3.58	-0.17	0.15	0.14	0.001	RAIL
248.191	40.781	-1.59	-0.10	0.14	0.13	0.001	RBUT
238.852	44.260	-0.27	2.59	0.14	0.13	0.002	REDM
238.272	46.768	2.47	3.63	0.47	0.54	-0.008	REFL
248.080	43.657	-2.34	-1.50	0.25	0.26	-0.020	RGBY
247.064	42.709	-2.66	-1.17	0.32	0.34	-0.051	RM55
242.761	46.045	0.19	0.02	0.47	0.50	0.010	RNDE
240.263	48.394	-0.40	0.63	0.64	0.70	-0.047	ROSW
238.931	48.734	2.35	1.52	0.40	0.40	-0.030	RSL2
245.706	43.747	-2.67	-0.73	0.31	0.36	-0.078	S014
248.764	44.801	-0.68	0.04	0.32	0.33	-0.035	S138
242.950	46.426	0.95	-0.67	0.47	0.56	-0.074	S262
239.930	48.157	0.80	0.91	0.39	0.45	-0.029	S389
243.202	44.445	-1.48	0.09	0.28	0.31	-0.048	S408
244.162	42.880	-2.72	-0.16	0.22	0.24	-0.021	S418
243.478	43.581	-2.04	-0.31	0.25	0.26	-0.022	S67A
239.523	46.602	0.54	1.89	0.32	0.37	0.045	SARG
240.662	47.185	0.38	0.45	0.35	0.38	-0.027	SAT3
247.399	44.897	-0.72	-0.19	0.59	0.60	0.005	SGCK
245.340	43.141	-2.93	-0.34	0.24	0.26	-0.008	SHAM
239.775	40.592	-6.51	3.86	0.14	0.13	-0.002	SHIN
240.984	41.868	-3.63	1.82	0.15	0.14	0.001	SHLD

Table S-9. Continued.

Longitude ºE	Latitude ºN	East Velocity (mm/yr)	North Velocity (mm/yr)	East Sigma (mm/yr)	North Sigma (mm/yr)	East-North Correlation	GPS Site
245.583	42.936	-2.85	-0.49	0.34	0.34	-0.008	SHOG
243.827	45.749	0.27	-0.17	0.34	0.40	-0.008	SKOO
250.377	42.855	-0.33	-0.31	0.50	0.55	0.075	SLIM
247.155	39.426	-3.17	-0.51	0.14	0.13	0.004	SMEL
243.824	47.546	-0.01	-0.28	0.47	0.54	-0.036	SMLT
246.117	45.114	-0.48	-1.36	0.27	0.29	-0.024	SMNA
244.413	36.320	-3.38	0.04	0.15	0.14	0.000	SMYC
247.873	39.306	-3.12	-0.06	0.18	0.17	0.002	SPIC
242.576	47.518	0.02	-0.57	0.20	0.19	0.001	SPN1
238.863	46.227	1.25	2.17	0.26	0.28	-0.006	SPR4
248.840	45.434	0.26	-0.77	0.58	0.67	0.083	SQUA
249.357	43.938	-1.30	-0.42	0.40	0.38	0.098	SRGP
307.322	47.595	-0.10	-0.86	0.64	0.64	0.009	STJO
307.322	47.595	-0.21	1.58	0.29	0.30	0.026	STJO
240.215	41.583	-4.18	2.15	0.52	0.57	0.003	STNN
238.330	45.305	0.90	3.91	0.69	0.76	0.005	STOL
240.937	45.004	-0.28	0.64	0.53	0.60	-0.006	STON
246.011	47.991	-0.02	-0.40	0.48	0.57	0.012	SWAN
247.740	45.061	-0.85	0.19	0.66	0.67	0.001	SWET
242.757	42.927	-3.17	0.17	0.64	0.76	-0.040	T128
244.136	43.816	-3.45	-0.07	0.35	0.41	0.057	T144
246.522	43.619	-2.58	-0.74	0.24	0.22	0.000	TCSG
239.549	46.626	2.67	1.46	0.63	0.64	-0.011	TERH
247.770	43.839	-2.10	-1.75	0.52	0.52	-0.004	TERI
244.898	42.087	-3.36	-0.41	0.26	0.28	-0.026	THR3
240.548	48.694	0.57	0.50	0.61	0.77	-0.035	TNSK
242.951	39.542	-4.06	0.20	0.18	0.17	0.002	TOIY
240.934	43.585	-1.94	1.26	0.46	0.48	-0.012	TOMB
242.816	38.097	-4.01	0.64	0.15	0.14	-0.001	TONO
249.403	43.674	-1.73	-1.09	0.17	0.15	0.000	TSWY
241.743	40.403	-5.28	1.46	0.15	0.14	0.001	TUNG
241.993	42.923	-2.86	0.53	0.29	0.31	-0.065	TURN
245.524	42.480	-2.91	-0.69	0.23	0.25	-0.035	TWFA
249.919	42.926	-0.34	-0.22	0.25	0.27	0.020	U044
248.195	43.836	-3.24	-1.78	0.26	0.20	-0.048	U11D
245.783	44.520	-1.41	-1.08	0.60	0.61	-0.007	U15A
244.110	42.466	-3.34	-0.54	0.62	0.63	0.000	U419
248.894	43.738	-2.50	-1.94	0.24	0.19	-0.047	U59A
239.782	44.631	-0.75	1.88	0.32	0.37	0.021	U73H
244.269	43.131	-2.88	-0.46	0.21	0.22	-0.003	U76A
241.042	45.138	-0.66	1.11	0.58	0.64	-0.023	UKIH
241.198	39.627	-6.41	2.68	0.11	0.10	-0.005	UPSA
244.442	43.490	-2.80	-0.31	0.24	0.25	-0.032	V162

Table S-9. Continued.

Longitude ºE	Latitude ºN	East Velocity (mm/yr)	North Velocity (mm/yr)	East Sigma (mm/yr)	North Sigma (mm/yr)	East-North Correlation	GPS Site
238.973	42.393	-3.66	4.63	0.59	0.72	-0.042	V357
238.122	42.574	-2.00	5.63	0.52	0.59	-0.038	V546
241.385	42.450	-3.02	1.60	0.63	0.64	-0.005	V696
243.697	45.566	-0.15	0.26	0.53	0.66	0.062	VERT
243.528	44.598	-1.08	0.02	0.41	0.53	-0.026	VOOM
249.066	42.707	-1.15	-0.46	0.27	0.28	0.009	W067
239.226	43.011	-2.96	3.48	0.52	0.60	-0.035	W072
241.717	46.088	-0.36	-0.08	0.36	0.39	-0.023	WALA
241.629	40.015	-5.88	2.11	0.45	0.48	-0.007	WCRK
288.507	42.613	0.25	0.14	0.29	0.29	0.014	WES2
248.408	44.902	-0.59	-2.42	0.60	0.63	0.003	WFRA
238.312	43.682	-1.34	4.03	0.72	0.76	-0.031	WKDM
245.970	43.433	-2.72	-0.55	0.54	0.53	0.018	WODI
247.212	46.184	-0.65	-0.97	0.27	0.30	-0.008	WSSB
246.148	44.204	-1.76	-0.22	0.41	0.47	0.052	X51X
246.665	41.565	-2.83	-1.30	0.48	0.51	0.003	X95X
238.865	45.233	0.18	2.25	0.37	0.42	-0.044	Y109
243.558	44.752	-0.84	-0.24	0.53	0.65	0.005	Y27X
245.415	47.833	0.47	-0.71	0.48	0.52	-0.004	Y382
243.709	45.656	0.13	0.17	0.50	0.52	-0.013	Y405
246.261	42.567	-3.33	-0.88	0.18	0.18	0.007	Y423
251.210	45.714	0.10	-0.51	0.53	0.51	0.090	Y538
245.519	62.481	-0.75	-1.52	0.16	0.14	-0.003	YELL
245.136	47.445	0.20	-0.26	0.60	0.80	0.070	Z140
242.112	48.541	0.48	0.04	0.56	0.58	-0.010	Z264
246.013	44.007	-2.61	-1.21	0.23	0.25	-0.026	Z425

References

Anders, M.H., Geissman, J.W., Piety, L.A. & Sullivan, J.T., 1989. Parabolic distribution of circumeastern Snake River Plain seismicity and latest Quaternary faulting: Migratory pattern and association with the Yellowstone Hotspot, *J. Geophys. Res.*, **94**, 1589-1621.

Byrd, J.O.D., Smith, R.B., & Geissman, J.W., 1994. The Teton fault, Wyoming: Topographic signature, neotectonics, and mechanisms of deformation, *J. Geophys. Res.*, **99**, 20095-20122.

Chang, W.-L., Smith, R.B., Wicks, C., Farrell, J.M. & Puskas, C.M., 2007. Accelerated uplift and magmatic intrusion of the Yellowstone Caldera, 2004-2006, *Science*, **318**, 952-956.

Chang, W.-L., Smith, R.B., Puskas, C.M., & Farrell, J.M., 2010. Kinematics and magmatic modeling of an extraordinary period of Yellowstone caldera uplift, 2004-2009, from GPS and InSAR observations, *Geophys. Res. Letts.*, **37**, L23302, doi:10.1029/2010GL045451.

Doser, D.I. & Smith, R.B., 1989. An assessment of source parameters of earthquakes in the Cordillera of the western United States, *Bull. Seis. Soc. Am.*, **79**, 1383–1409.

Holmes, A.A.J., Rodgers, D.W. & Hughes, S.S., 2008. Kinematic analysis of fractures in the Great Rift, Idaho: Implications for subsurface dike geometery, crustal extension, and magma dynamics, *J. Geophys. Res.,* **113**, B04202, doi:10/1029/2006JB004782.

Jackson, S.M., Wong, I.G., Carpenter, G.S., Anderson, D.M. & Martin, S.M., 1993. Contemporary seismicity in the eastern Snake River Plain, Idaho based on microearthquake monitoring, *Bull. Seis. Soc. Am.*, **83**, 680–695.

Jackson, S.M. & Zollweg, J.E., 1988. Seismic studies of an earthquake sequence in the White Cloud Peaks, Idaho, *Seis. Res. Lett.*, **59**, 6.

Kuntz, M.A., Spiker, E.C., Rubin, M., Champion, D.E. & Lefebvre, R.H., 1986. Radiocarbon studies of latest Pleistocene and Holocene Lava flows of the Snake River Plain, Idaho: Data, lessons, interpretations, *Quaternary Res.*, **25**, 163-176.

Kuntz, M.A., Covington, H.R., & Schorr, L.J., 1992. An overview of basaltic volcanism of the eastern Snake River Plain, Idaho, in Link, P. K., Kuntz, M. A. & Platt, L. B., eds., Regional Geology of Eastern Idaho and Western Wyoming, *Geol. Soc. Am. Memoir,* **179**, 227-267.

Kuntz, M.A., Anderson, S.R., Champion, D.E., Lanphere, M.A. & Grunwald, D.J., 2002. Tension cracks, eruptive fissures, dike, and faults related to late Pleistocene – Holocene basaltic volcanism and implications for the distribution of hydraulic conductivity in the eastern Snake River Plain, Idaho, in Link, P.K. and L.L. Mink, eds., Geology, Hydrogeology, and Environmental Remediation: Idaho National Engineering and Environmental Laboratory, Eastern Snake River Plain, Idaho, *Geol. Soc. Am. Special Paper,* **353**, 111-133.

Kuntz, M.A., Skipp, B., Champion, D.E., Gans, P.B., Van Sistine, D.P. & Snyders, S.R., 2007, Geologic map of the Craters of the Moon 30' x 60' quadrangle, Idaho, *U.S. Geol. Survey Sci. Investigation Map*, **SIM-2969**, scale 1:100,000.

McCaffrey, R., 2005. Block kinematics of the Pacific – North America plate boundary in the southwestern US from inversion of GPS, seismological, and geologic data, *J. Geophys. Res.*, **110**, B07401, doi:10.1029/2004JB003307.

McCaffrey, R., 2009. Time-dependent inversion of three-component continuous GPS for steady and transient sources in northern Cascadia, *Geophys. Res. Letts.*, **36**, L07304, doi:10.1029/2008GL036784.

McCaffrey, R., Qamar, A.I., King, R.W., Wells, R., Khazaradze, G., Williams, C.A., Stevens, C.W., Vollick, J.J. & Zwick, P.C., 2007. Fault locking, block rotation and crustal deformation in the Pacific Northwest, *Geophys. J. Int.*, 169, 1315-1340.

Nishimura, T. & Thatcher, W., 2003. Rheology of the lithosphere inferred from postseismic uplift following the 1959 Hebgen Lake earthquake, *J. Geophys. Res.*, **108**, 2389, doi:10.1029/2002JB002191.

Payne, S.J., McCaffrey, R. & King, R.W., 2009. Time-dependent inversion of three-component continuous GPS for steady and transient effects of the Yellowstone Hotspot on the Snake River Plain, Idaho, *EOS Trans. Am. Geophys. Union*, **90** (52), Fall Meet. Suppl. G33A-0622.

Pezzopane, S.K. & Weldon, R. J., 1993. Tectonic role of active faulting in central Oregon, *Tectonics*, **12**, 1140-1169.

Pierce, K.L. & Morgan, L.A., 1992. The track of the Yellowstone hotspot: Volcanism, faulting, and uplift; in Link, P. K., Kuntz, M. A., and Platt, L. B., editors, Regional Geology of Eastern Idaho and Western Wyoming, *Geol. Soc. Am. Memoir,* **179**, 1-53.

Pollitz, F.F., 1992. Postseismic relaxation theory on the spherical Earth, *Bull. Seismol. Soc. Am.,* **82**, 422-453.

Richins, W.D., Pechmann, J.C., Smith, R.B., Langer, C.J., Goter, S.K., Zollweg, J.E. & King, J.J., 1987. The 1983 Borah Peak, Idaho earthquake and its aftershocks, *Bull. Seis. Soc. Am.*, **77**, 694-723.

Smith, R.B. & Braile, L.W., 1993. Topographic signature, space-time evolution, and physical properties of the Yellowstone-Snake River Plain volcanic system: The Yellowstone hotspot, in Snoke, A.W., Steidtmann, J. & Roberts, S.M., eds., Geology of Wyoming, *Geological. Survey of Wyoming Memoir,* **5**, 694-754.

Stein, S. & Gordon, R.G., 1984. Statistical tests of additional plate boundaries from plate motion inversions, *Earth Planet. Sci. Lett.*, **69**, 401-412.

Stickney, M.C., 1997. Seismic source zones in southwestern Montana, *Montana Bureau of Mines and Geology Open-File Report,* **366**, 52 p.

Stickney, M.C., 2007. Historic earthquakes and seismicity in southwestern Montana, *Northwest Geology*, **36**, 167-186.

Thackray, G.D., Rodgers, D.W., Johnson, E.M., & Shapley, M.D., 2009. Preliminary evaluations of a newly discovered Holocene scarp on the Sawtooth fault, centeral Idaho, *Geol. Soc. Am. Abstracts with Programs*, **41**, 55.

Wood S.H., & Clemens, T., 2002. Geologic and tectonic history of the Western Snake River Plain, in Bonnichsen, B., White, C.M. & McCurry, M., eds., Tectonic and magmatic evolution of the Snake River Plain volcanic province, Idaho, *Idaho Geological Survey Bulletin,* **30**, 69-103.

Zollweg, J.E. & Richins, W.D., 1985. Later aftershocks of the 1983 Borah Peak, Idaho earthquake and related activity in central Idaho, in Proc. Workshop XXVIII on the 1983 Borah Peak, Idaho, earthquake, *U.S. Geol. Surv. Open-File Report,* **85–290**, 345-367.